Non-congruence of high-temperature mechanical and structural behaviors of $LaCoO_3$ based perovskites – ACCEPTED 03.11.16

Amjad Aman[1], Ryan Jordan[1],Yan Chen [1,2], Richard Stadelmann[1], Mykola Lugovy[1,3], Nina Orlovskaya[1*], E. Andrew Payzant [2], Clarina dela Cruz[4], Michael J. Reece[5], Thomas Graule[6], Jakob Kuebler[6]

[1]Department of Mechanical and Aerospace Engineering, University of Central Florida, Orlando, Florida 32816, USA

[2]Chemical and Engineering Materials Division, Oak Ridge National Laboratory, Oak Ridge, Tennessee 37831, USA

[3]Institute for Problems of Materials Science, Kiev, Ukraine

[4]Quantum Condensed Matter Division, Neutron Sciences Directorate, Oak Ridge National Laboratory, Oak Ridge, Tennessee 37831, USA

[5]The School of Engineering and Materials Science, Queen Mary, University of London, London, UK

[6]Empa, Swiss Federal Laboratories for Materials Science and Technology, Laboratory for High Performance Ceramics, Ueberlandstrasse 129, 8600 Duebendorf, Switzerland

* Corresponding author: email Nina.Orlovskaya@ucf.edu
Phone: 1-407-913-4438. Address: 4000 Central Florida Blvd., Orlando, Fl 32816

Abstract

This paper presents the mechanical behavior of $LaCoO_3$ and $La_{0.8}Ca_{0.2}CoO_3$ ceramics under four-point bending in which the two cobaltites are subjected to a low stress of ~8 MPa at temperatures

ranging from room temperature to 1000 ^{o}C. Unexpected stiffening is observed in pure $LaCoO_3$ in the 700-900 ^{o}C temperature range, leading to a significant increase in the measured Young's modulus, whereas $La_{0.8}Ca_{0.2}CoO_3$ exhibits softening from 100 ^{o}C to 1000 ^{o}C, as it is expected for most materials upon heating. Neutron diffraction, X-ray diffraction and micro-Raman spectroscopy are used to study the crystal structure two materials in the RT-1000 ^{o}C temperature range. Despite a detailed study, there is no conclusive evidence to explain the stiffening behavior observed in pure $LaCoO_3$ as opposed to the softening behavior in $La_{0.8}Ca_{0.2}CoO_3$ at high temperatures (above 500 ^{o}C).

Key words:

Lanthanum cobaltite, powder diffraction, Raman spectroscopy, Young's modulus, temperature dependence, hysteresis.

1. INTRODUCTION

Mixed Ionic Electronic Conducting (MIEC) $LaCoO_3$ based perovskites have been studied very extensively due to their unique and distinctive electronic, electrochemical, catalytic, and mechanical properties [1-8]. It was reported that polycrystalline $LaCoO_3$ based perovskites exhibit nonlinear ferroelastic behavior, which can be well explained by the kinetics of ferroelastic switching and corresponding changes in the cobaltite's microstructure and crystallographic orientation during loading [9]. The phenomena of domain switching and texture development were reported to be responsible for the appearance of elastic anisotropy and stress-strain hysteresis during deformation [9, 10]. It was also reported that at room temperature both pure $LaCoO_3$ and Ca doped $LaCoO_3$ have $R\bar{3}c$ low symmetry rhombohedral structure with a=5.378 Å and α=60.8^{o}

for pure $LaCoO_3$, and a=5.374 Å and α=60.72° for 20% Ca doped $LaCoO_3$, which is in perfect agreement with previously reported measurements [11-13]. Upon heating, the rhombohedral distortion in the lattice gradually decreases along with an increase in the lattice parameters up to the temperature at which a phase transition takes place to the high symmetry $Pm\bar{3}m$ cubic structure. Doping $LaCoO_3$ with cations like Ca^{2+} is known to reduce the lattice distortion and lower the transition temperature [14]. The $R\bar{3}c$ to $Pm\bar{3}m$ phase transition has been reported to occur above 1200°C for pure $LaCoO_3$ and at ~950°C for $La_{0.8}Ca_{0.2}CoO_3$, corresponding to the fact that a greater rhombohedral distortion at room temperature results in a higher transition temperature to cubic structure [14]. It is also know that the transition from the higher symmetry paraleastic phase to the lower symmetry ferroelastic phase leads to distortion in the cubic lattice, which results in spontaneous strain, and hence the lower symmetry phase has a non-linear deformation behavior. While only $R\bar{3}c$ rhombohedral structure was found at room temperature using most diffraction techniques, the existence of the lower symmetry monoclinic I2/a phase in $LaCoO_3$ based perovskite was confirmed by TEM and high-resolution synchrotron diffraction experiments. It is hard to detect in general by normal X-ray and neutron diffraction techniques due to the fact that the monoclinic distortion is very small and there are peaks overlapping peaks [15-17]. Vullum et al. also reported the presence of a monoclinic phase in $LaCoO_3$, even though they reported the monoclinic space group as $P2_1/m$ [18, 19].

It is important to mention that in our previous investigation of the thermal and mechanical properties of $LaCoO_3$ and $La_{0.8}Ca_{0.2}CoO_3$, a very unusual behavior was observed for pure lanthanum cobaltite [11]. At high temperatures (700-1000°C), $La_{0.8}Ca_{0.2}CoO_3$ perovskite exhibits significant softening as expected and the value of Young's modulus decreases in comparison with the value at room temperature. On the other hand, pure $LaCoO_3$ exhibits an unexpected increase

in Young's modulus with temperatures, varying from 76GPa at room temperature to 120GPa at 800°C, a 30% increase in magnitude, while the lattice continuously expands from room temperature to 1000°C as reported in [11]. The Young's modulus of $LaCoO_3$ and $La_{0.8}Ca_{0.2}CoO_3$ perovskites was measured from the loading portions of the stress-strain deformation curves obtained during 4-point bending experiments. The stiffening of $LaCoO_3$ reported in [11] was not explained and no detailed investigation into the unusual phenomenon was performed. In a paper by Raccah and Goodenough, the high temperature phase transition in $LaCoO_3$ was reported [20], however, these results were retracted in a later publication [12], where the explanation of the phase transition in $LaCoO_3$ was replaced by the appearance of the secondary Co_3O_4 oxide spinel phase as an impurity in $LaCoO_3$, thus leading to the disruptive changes in measured lattice parameters, that were erroneously assigned to the first order phase transition in $LaCoO_3$.

A summary of the many published results that have reported the variation of Young's modulus with temperature in different MIEC perovskites, all of them being of high relevance for their use in solid oxide fuel cells, was presented in [21]. This rather comprehensive review revealed that for certain perovskite compositions under certain experimental conditions, the Young's modulus decreases in the 100-600°C temperature range and then increases in the 700-1000°C temperature range [22, 23], while other materials with different perovskite compositions under similar or different experimental conditions showed the expected softening upon heating to 1000°C [24, 25]. A significant softening of $La_{0.8}Sr_{0.2}FeO_{3-\delta}$ and $La_{0.8}Sr_{0.2}Fe_{0.7}Ga_{0.3}O_{3-\delta}$ in the 200-400°C temperature range followed by an increase in the Young's modulus at 700-900°C was reported in [23]. The phase transition occurring in the 700-900°C temperature range was considered to be responsible for the stiffening of the material in the higher temperature range (700-900°C) in $LaCoO_3$ based ceramics [23]. Similar softening followed by a small stiffening behavior of

$La_{0.9}Sr_{0.1}Ga_{0.8}Mg_{0.2}O_{3-\delta}$ during heating to 1100°C was attributed to the successive structural changes in this perovskite material [26]. Changes both in Young's and shear moduli reported in [26] lead to the appearance of a significant discontinuity in the Poisson's ratio of $La_{0.9}Sr_{0.1}Ga_{0.8}Mg_{0.2}O_{3-\delta}$ at 600°C. A significant increase in measured Young's modulus of dense $La_{0.8}Sr_{0.2}MnO_3$ perovskite ceramics was reported to occur in the 600-1000°C temperature range, while no change in Young's modulus was found for the same composition when the ceramics had low density and an open pore structure [22]. A very large increase in Young's modulus of $La_{1-x}Sr_xMnO_3$ at high temperatures was also reported [21]. The variation of Young's modulus with temperature for $La_{0.58}Sr_{0.4}Co_{0.2}Fe_{0.8}O_{3-\delta}$ was reported in [27], and an attempt at explaining the phenomenon by phase transition is covered in [28]. Similar stiffening of other mixed ionic electronic conducting ceramics was found in [22], where an increase in Young's modulus of $LaMnO_3$ and $LaFeO_3$ based perovskites in the 800-1000°C temperature range was reported, however, again, no reasonable explanations were provided to explain this behavior.

In the current paper, the significant increase in Young's modulus of $LaCoO_3$ in the 700-1000°C temperature range is reported, as measured using stress-strain deformation plots in four-point bending and sample resonance using the impulse excitation technique. For comparison, the properties of $La_{0.8}Ca_{0.2}CoO_3$ perovskite were also measured. Since the cobaltites exhibit non-linear deformation behavior upon loading, even at very small stresses, the Young's modulus cannot simply be directly determined from stress-strain data. Therefore, in the case of the four-point bending measurements the term "Young's modulus" will be replaced by the term "effective Young's modulus" in the paper. The detailed study of crystal structure of the two cobaltite compositions were done using powder X-ray diffraction as well as neutron diffraction.

2. EXPERIMENTAL

The $LaCoO_3$ and $La_{0.8}Ca_{0.2}CoO_3$ samples were sintered by Praxair Surface Technologies, Specialty Ceramics, USA; and machined by PremaTech Ceramics, USA. Three separate sample geometries were prepared – bars with dimensions 3mm x 4mm x 50mm for four-point bending experiments, bars with dimensions 50mm x 14mm x 14mm for impulse excitation measurements, and cylindrical pellets with 6mm diameter and 12mm length for compression testing.

The four-point bending tests of $LaCoO_3$ and $La_{0.8}Ca_{0.2}CoO_3$ samples were carried out at Empa, Swiss Federal Laboratories for Materials Science and Technology, Laboratory for High Performance Ceramics, Switzerland. The samples were loaded with a 20 mm loading span and 40 mm supporting span. A Universal Testing Machine (UPM-Zwick 1478, Germany) was used for testing, in accordance with EN 843-1 standard [29]. The heating and cooling rate was set at 15^{o}C/min, with a dwell time of 10 minutes for each temperature. The loading/unloading of the cobaltites was done up to a relatively small load to ensure that the maximum normal stress imposed on the sample during loading would be limited to ~8 MPa. As mentioned earlier, since the cobaltites exhibit non-linear deformation behavior, the ”true” Young’s modulus cannot be directly determined. Therefore, a method was adopted to estimate the “effective Young’s modulus” of the ceramics, the secant modulus from the force-displacement data. The secant modulus is defined as the slope of the straight line joining any given point in the stress-strain diagram to the origin. To estimate the effective Young’s modulus, first, the Secant modulus was plotted against applied stress. Then, the intercept of secant modulus-applied stress curve with the Secant modulus axis was considered as the effective Young’s modulus.

In addition, the Impulse Excitation Technique (IET) was used to determine the elastic modulus of the two materials for the same temperature range and intervals. The instrument used

is a Grindo-Sonic Mk5 "Industrial" (J.W. Lemmens, Belgium), and the measurements were carried out in accordance with the EN 843-2 standard [30]. Samples, in the form of bars, of known density were lined up with a supporting cylinder and placed over a microphone. To determine the elastic modulus at room temperature using the natural frequency of vibration, the test bar was struck slightly using a small hammer and the acoustic vibrations were recorded using the microphone. Then using the dimensions of the sample, its density and natural frequency of vibration, the Young's modulus was calculated. An electric furnace was used to heat the samples in air to the desired temperatures, with a dwell time of 30 minutes at each temperature. The samples were placed on a sample holder in the furnace and fixed with weights, and the microphone was again placed below the sample holder, and a similar procedure was followed to determine the elastic modulus at high temperatures. Instead of a small hammer, ZrO_2 or stainless steel balls with 4mm diameter were used to excite the samples.

Powder diffraction of the $LaCoO_3$ and $La_{0.8}Ca_{0.2}CoO_3$ samples was conducted using neutron diffraction and X-ray diffraction (XRD) techniques. All of the collected diffraction data were analyzed by Rietveld refinement using the General Structure Analysis System (GSAS) software [31] along with the graphical user interface (EXPGUI) [32]. The $LaCoO_3$ and $La_{0.8}Ca_{0.2}CoO_3$ samples used for these experiments were in the form of powders ground from the sintered cylindrical pellets.

The neutron powder diffraction experiments were conducted at the Spallation Neutron Source (SNS) and High Flux Isotope Reactor (HFIR) facilities at Oak Ridge National Laboratory (ORNL). At SNS the beamline 11A called POWGEN was utilized, which is a general-purpose powder diffractometer with a relatively high resolution of $0.001 < \Delta d/d < 0.016$. The powder samples were loaded into a quartz basket and placed in an air furnace. The temperature was raised

from 100 ^{o}C to a maximum of 820 ^{o}C, and the diffraction data were collected at each designed temperature dwell for 0.5~1 h. The wavelength center of the neutrons was set at 1.333 Å, such that the time-of-flight neutron diffraction patterns covered a *d*-spacing range of 0.41 to 3.61 Å.

The experiment at HFIR was conducted on the HB-2A High Resolution Neutron Powder Diffractometer. The HB-2A is an instrument that is helpful in crystal structural studies under varying conditions like pressure and temperature, and helps determine atomic positions, atomic displacement, atomic occupancies and phase transition. The HB-2A has a bank of 44 ^{3}He tubes, each with 12' Soller collimators arranged in a Debye-Scherrer geometry. The monochromator used is a Ge [115] corresponding to a wavelength of 1.1538 Å. The sample in the form of a pellet of 6mm diameter, 12 mm length was heated in a quartz tube within an air furnace. Quartz wool was placed on top of the sample to avoid any contamination from escaping out into the environment. Two thermocouples were used to monitor the sample and environment temperatures. The temperature of the sample was varied from 200^{o}C to 1050^{o}C in intervals of about 50^{o}C; a scan at 11^{o}C was also conducted. The time allotted for the temperature of the samples to stabilize was 20 minutes for each temperature. The time required per scan was approximately 68 minutes.

The high temperature X-ray diffraction was conducted at the High Temperature Materials Laboratory (HTML) at ORNL using a PANalytical X'Pert PRO MPD diffractometer with an Anton-Paar XRK-900 high temperature stage. Powder diffraction was performed for cylindrical samples. The data was collected in the 2θ range of 10^{o}-80^{o} with a count time of 30 seconds resulting in a scan duration of less than 5 minutes, using Cu Kα radiation at 45 kV and 40mA. The use of an X'celeraotor detector allowed fast data collection.

3. RESULTS AND DISCUSSION

Stress-strain curves of $LaCoO_3$ and $La_{0.8}Ca_{0.2}CoO_3$ ceramics obtained under uniaxial compression are shown in Fig. 1. Both materials exhibit ferroelastic hysteresis, which was well characterized in our previous work [8, 9, 33, 34]. The inserts in Fig. 1 show stress-strain plots obtained both in uniaxial compression during loading (dashed line) and, for comparison, in four point bending during loading/unloading up to 8 MPa (solid line) and shows a good overlap of the data from the two tests.

The stress-strain hysteresis plots of $LaCoO_3$ and $La_{0.8}Ca_{0.2}CoO_3$ as a function of temperature for heating and cooling are shown in Fig. 2. Hysteresis loops were obtained in both perovskites at almost all temperatures with the only exception that an almost straight line and no hysteresis is visible for loading/unloading of $La_{0.8}Ca_{0.2}CoO_3$ at room temperature. The characteristic features of hysteresis of $LaCoO_3$ and $La_{0.8}Ca_{0.2}CoO_3$ on loading/unloading at different temperatures obtained from the results presented in Fig. 2 are presented in Fig. 3. The hysteresis area of $LaCoO_3$ is larger in comparison with Ca doped $LaCoO_3$ at room temperature as well as at 100^{o}C (Fig. 3A and B). However, beginning at 200^{o}C there is a significant increase in the hysteresis area measured for Ca doped cobaltite, when the values of hysteresis area increase to almost 300 Pa upon heating, whereas for pure $LaCoO_3$ an increase of hysteresis area was also detected but the values at 200^{o}C were in the range of 100 Pa both upon heating and cooling, which is three times less than those of Ca doped $LaCoO_3$. The trend shows an increase in the hysteresis area between 200^{o}C to ~400^{o}C for both compounds, and then a decrease up to 800^{o}C, followed by a slight increase in the value for $LaCoO_3$ and a large increase for Ca doped $LaCoO_3$. The largest area of hysteresis loop was measured for $La_{0.8}Ca_{0.2}CoO_3$ at 1000^{o}C when plastic deformation, most likely caused by the movement of dislocations, was present (Fig. 2C and D). Other parameters, such as irreversible strain, showed similar trends for pure and Ca doped $LaCoO_3$ (Fig. 3C and D). Both hysteresis areas

and irreversible strains increased in the 200-400°C temperature range for both compositions. Both hysteresis areas and irreversible strains slightly decreased in the 700-1000°C temperature range for pure $LaCoO_3$, however in the 600-700°C temperature range the hysteresis area, irreversible and even maximum strains decreased for Ca doped $LaCoO_3$, while at the higher 900-1000°C temperature range, especially at 1000°C, all three parameters increased dramatically for $La_{0.8}Ca_{0.2}CoO_3$ (Fig. 3E and F). The effective Young's modulus of both compounds showed contrasting behavior upon heating (Fig. 3G and H). As the effective Young's modulus strongly depends on the bond strength and bond length of the compound, as temperature increases the bond strength decreases as the bond length increases, thus bringing down the stiffness of the bonds causing the expected softening of the material at high temperature. The effective Young's modulus of $LaCoO_3$ remains equal to ~80 GPa at room temperature and at 100°C, the perovskite slightly softens at 200-400°C until the value reaches ~75 GPa. However, starting from 600-700°C the effective Young's modulus value increases close to 120 GPa at 800°C (Fig. 3G). The effective Young's modulus values measured from the loading portion of the stress-strain deformation plot taken at the very beginning of the loading and the Young's modulus measurements taken from impulse excitation technique coincide well (Fig. 3G). However, for $La_{0.8}Ca_{0.2}CoO_3$, the effective Young's modulus behavior is very different from the behavior of pure $LaCoO_3$ upon heating (Fig. 3H). As can be seen in Fig. 3H, the effective Young's modulus of $La_{0.8}Ca_{0.2}CoO_3$ is ~135 GPa both at room temperature and 100°C, but upon further increase in temperature the effective Young's modulus decreases to ~50 GPa at 1000°C, exhibiting the expected softening behavior. Thus, unusual stiffening behavior of $LaCoO_3$ where effective Young's modulus increases significantly upon increase of temperature, is observed and needs to be understood.

While there have been many studies done of the crystal structure, phase composition, lattice

parameters and other aspects including Co ion spin states of $LaCoO_3$ using neutron diffraction and X-ray diffraction in the past [35-38], the purpose of this study was to present an even more comprehensive high temperature neutron and X-ray diffraction study to clarify the changes in the crystal structure and lattice parameters of both pure and Ca doped $LaCoO_3$. The room temperature neutron and X-ray diffraction patterns of LaCoO3 and La0.8Ca0.2CoO3 perovskites are shown in Fig. 4. The refinement results from powder diffraction patterns taken on the HB-2A instrument at HFIR and POWGEN instrument at SNS at ORNL coincide well with the X-ray diffraction (XRD) patterns taken using the X-ray diffractometer at the High Temperature Materials Laboratory at ORNL. Only peaks belonging to $LaCoO_3$ based perovskite structure were indexed and thus phase pure rhombohedral $R\bar{3}c$ structure was identified; a schematic of the unit cell and bonds in the cobaltite's lattice are shown in Fig. 5. Both rhombohedral and hexagonal lattice unit cells are shown in Fig. 5A and B, as well as the characteristic bond lengths of Co-O and La-O, as seen in Fig. 5C and D respectively. The O-Co-O bond angle (Fig. 5C), O-La-O bond angle (Fig. 5D) and the Co-O-Co angle (Fig. 5E) between two octahedrons are also shown. The diffraction patterns of pure $LaCoO_3$ and $La_{0.8}Ca_{0.2}CoO_3$ perovskites taken at different temperatures are shown in Fig. 6. Peaks that belong to only the rhombohedral $R\bar{3}c$ structure are observed and lattice expansion is observed as the temperature increases. Examples of Rietveld refinement results for $LaCoO_3$ are shown at 11°C (Fig. 7A) and 1000°C (Fig. 7C), and for $La_{0.8}Ca_{0.2}CoO_3$ are shown at 11°C (Fig. 7B) and 1000°C (Fig. 7D) from data collected at HFIR. The fitting parameters wRp, Rp and reduced $\chi 2$ were found to be in the range of 3.9%–5%, 3.1%–4% and 0.84–1.3, respectively The rhombohedral *a* and *c* lattice parameters as well as the volume of the unit cell as a function of temperature are shown in Fig. 8. There is good correspondence between lattice parameters and volume of the two compounds as measured by three different methods – two of them by neutron

diffraction and one by X-ray diffraction. The smooth evolution of lattice parameters and cell volume as a simple thermal response of the lattice indicates the absence of phase transition in the two materials. It is possible to see from the corresponding lattice parameters, that the thermal expansion and increase in "*a*" lattice parameter was much larger for pure $LaCoO_3$ in comparison with $La_{0.8}Ca_{0.2}CoO_3$. As one can see from Fig. 8A and D, the "*a*" lattice parameters are rather similar at room temperature for both compounds (5.37-5.38 Å) but there is a difference at high temperatures - 5.537±0.00117 Å for $LaCoO_3$ and 5.505±0.00100 Å for $La_{0.8}Ca_{0.2}CoO_3$ at 1000ºC. There is no indication of any significant changes in the thermal expansion of $LaCoO_3$ which might correlate and account for the measured increase in effective Young's modulus of this compound. The change in the rhombohedral angle with temperature of the two compounds reveals that $La_{0.8}Ca_{0.2}CoO_3$ perovskite has a ferroelastic phase transition at ~1050ºC with $\alpha=60^{o}\pm0.005^{o}$ ($\alpha=60^{o}$ for cubic phase), whereas $LaCoO_3$ is still rhombohedral ($\alpha=60.18^{o}\pm0.009^{o}$) even at 1050ºC (Fig. 8).

There are significant differences in the variation of Co-O, La-O bond lengths and O-Co-O, Co-O-Co, O-La-O bond angles with temperature, between pure $LaCoO_3$ and $La_{0.8}Ca_{0.2}CoO_3$ compositions (Fig. 9 and 10). Co-O and La-O bond lengths increase much faster in pure $LaCoO_3$ upon heating in comparison with $La_{0.8}Ca_{0.2}CoO_3$. The O-Co-O bond angle approaches 90º at 1100ºC for $La_{0.8}Ca_{0.2}CoO_3$ indicating that the structure becomes close to cubic, whle for pure $LaCoO_3$ the structure still has a significant distortion and remains rhombohedral at all temperatures. The geometric tolerance factor approaches 1 for $La_{0.8}Ca_{0.2}CoO_3$ at 1050ºC, but for pure $LaCoO_3$ it is remains at 0.996. Thus, despite the significant increase in effective Young's modulus of pure $LaCoO_3$ at 700-900ºC, the lattice expansion and bond lengths/angles do not provide any clear answer as to why the effective Young's modulus increases.

Refinement for oxygen occupancies for the two compounds from neutron diffraction results was inconclusive. There was no discernable trend as far as the amount of oxygen vacancies as a function of temperature that can be inferred, as seen in Fig. 11 (A, B). The Atomic Displacement Parameter, presented as U_{iso} for isotropic case in the refinement, characterizes the thermal vibration of the oxygen atoms, plotted against temperature for the two compounds as shown in Fig. 11 (C, D). It is expected to have a higher value at elevated temperatures due to stronger thermal vibrations. However, the value can be also high if the structure locally involves incoherent static distortions [39] of the CoO_6 octahedra. The incoherent atomic displacements with respect to the lattice-averaged positions may not contribute to additional Bragg's reflection, but will mimic large Debye-Waller factors. This effect is hard to differentiate from that owing to the thermal vibrations in the diffraction patterns. From the plots in Fig. 11 (C, D), there is a change in slope for $LaCoO_3$ at about 500^{o}C, which coincides with the temperature at which there is an increase in its effective Young's modulus. In contrast, there is no change in slope for $La_{0.8}Ca_{0.2}CoO_3$ that can be observed, and the effective Young's modulus continues to decrease with increasing temperature. Therefore, it is proposed that at high temperatures, some static distortions occur in $LaCoO_3$ but not in $La_{0.8}Ca_{0.2}CoO_3$. With the local static distortions, the atom's position can differ from the lattice-averaged sites, and therefore the true bond lengths cannot be precisely calculated from the "characteristic bond lengths" by the refinement. The subtle static distortions changes indicated by U_{iso} parameter lead to the variation in local bond lengths (true bond lengths) and may be responsible for the effective Young's modulus increase. Nevertheless, this mechanism cannot be fully verified by the current data. The change in local bond lengths could also be explained by the different valence and spin states of Co atoms. For these effects different directions, locally, there may be multiple modes of Co-O_6 octahedron distortions in the perovskite.

These are possible mechanisms, although not explicit, that could explain the effect that static distortions have on the anomalous behavior of U_{iso} with temperature in $LaCoO_3$.

From the X-ray and neutron diffraction analysis, the structure of $LaCoO_3$ based perovskites was identified as rhombohedral $R\bar{3}c$ (D_{3d}^6) structure, and according to the factor group analysis for D_{3d}^6 rhombohedral perovskites only five Raman active phonon modes of irreducible representation $A_{1g}+4E_g$ are allowed [40]. It was found in the previous work [41] that there are five active Raman peaks in pure $LaCoO_3$ when measurements were taken from the as-machined surface. When the sample is heated up to 900°C the effect of the strain at the surface associated with machining disappears [42]. Raman spectra were collected for the two compositions during heating from room temperature up to 900°C, and cooling back down to room temperature, as shown in Fig. 12 and Fig. 13. In Fig. 12, two low frequency modes 160 cm^{-1} (1) and 185 cm^{-1} (2) are present in the low frequency region, and two intermediate frequency modes 450 cm^{-1} (3) and 550 cm^{-1} (4), along with a strong 700 cm^{-1} (5) mode are detected for pure $LaCoO_3$. All of these peaks remain present on heating up to 900°C for both $LaCoO_3$ and $La_{0.8}Ca_{0.2}CoO_3$. The peak intensities decrease and peak widths increase upon heating to 900°C. For $LaCoO_3$ the 450 cm^{-1} and 550 cm^{-1} peaks, even as they weaken, remain separate even at 900°C; in contrast to $La_{0.8}Ca_{0.2}CoO_3$ for which the 450 cm^{-1} peak slowly disappears upon heating and only the 550 cm^{-1} could be seen at 900°C. There are two other important differences in the Raman spectra of pure and Ca-doped $LaCoO_3$. First, for the $La_{0.8}Ca_{0.2}CoO_3$ perovskite there is only one 185 cm^{-1} peak present in the low frequency region, as can be seen in Fig. 13. Second, for Ca-doped $LaCoO_3$ the 400 cm^{-1} (3') peak is more clearly present at room temperature and then weakens, but for pure $LaCoO_3$ the 400 cm^{-1} peak is hardly seen at room temperature but it becomes more prominent in the temperature range of 200-400°C. To summarize, there is no significant change in the Raman

spectra that could be indicative of any structural changes that would provide a realistic explanation as to why effective Young's modulus of $LaCoO_3$ increases so dramatically upon heating.

One of the possible explanations for the increase of effective Young's modulus of pure $LaCoO_3$ could be connected to the strong elastic anisotropy of this compound. As it was established in [10], a strong texture formed during the loading of this perovskite at room temperature, when the volume of the domains with a higher elastic modulus along loading direction increased thus leading to an increase in observed effective Young's modulus. Increase in temperature could bring about a significant increase in the mobility of the domain walls and, therefore, formation of texture might easily be facilitated, resulting in an increase in the effective Young's modulus at much lower applied stress, such as for example 8 MPa as it was applied in the current study. By providing such explanation though, one has to take precaution – the increase in temperature of the material not only allows for texture formation process to occur, but the increase in temperature also leads to decrease in the elastic constants that occurs simultaneously which leads to a reduction in the effective Young's modulus. The overall changes in effective Young's modulus would depend on these two processes – increase in the volume of the domains with a certain crystallographic orientations along the load direction as well as changes in the elastic constants – as a function of temperature. The use of the domain switching phenomenon to explain the variation of Young's modulus at high temperatures for other perovskites such as $La_{0.58}Sr_{0.4}Co_{0.2}Fe_{0.8}O_{3-\delta}$ was also found in [43].

Another factor that could contribute to the stiffening or softening behavior in the two compounds is the pinning effect of oxygen vacancies on the movement of domain walls. It has been reported that in perovskites such as $Ca_{1-x}Sr_xTiO_3$, oxygen vacancies or clusters of oxygen vacancies pin the domain walls, thus impeding the movement of domain walls and softening of

the material [44-46]. In Ca-doped $LaCoO_3$, the number of oxygen vacancies is higher due to doping with Ca and the number of vacancies should increase with temperature as more oxygen atoms leave the lattice at higher temperature, the density of clusters of oxygen vacancies is thus predictably much higher at high temperatures compared to pure $LaCoO_3$, thus the pinning effect of these clusters and the eventual softening that occurs could be much more significant in Ca-doped $LaCoO_3$, whereas in pure $LaCoO_3$ the mobility of the domain walls can still be the dominating phenomenon. This means that the domain wall mobility phenomenon dominates and leads to stiffening in pure $LaCoO_3$, and for Ca-doped $LaCoO_3$ the pinning effect due to large number of oxygen vacancy clusters dominates and leads to softening. To verify such hypotheses in-situ stress-strain X-ray or neutron diffraction experiments would be required, and this might be a subject of future work.

4. CONCLUSIONS

The stress-strain deformation behavior of $LaCoO_3$ and $La_{0.8}Ca_{0.2}CoO_3$ was studied by loading the ceramics to a low stress of 8 MPa in four-point bending at RT – 1000 ^oC temperature range. The changes in hysteresis loops were significant in the 200-500 ^oC range and at 1000 ^oC for both $LaCoO_3$ and $La_{0.8}Ca_{0.2}CoO_3$, however, the changes in the hysteresis loop area for $La_{0.8}Ca_{0.2}CoO_3$ was much more substantial. A very unusual phenomenon was noticed in $LaCoO_3$ – significant stiffening of the ceramic in the 700-900 ^oC temperature range. The effective Young's modulus of $LaCoO_3$ at room temperature was recorded as ~76 GPa, however, its value increased dramatically beginning around 700 ^oC to a value of ~120 GPa at 900 ^oC. In the case of $La_{0.8}Ca_{0.2}CoO_3$, softening behavior was recorded, as in the case for most materials, under the same testing conditions. High temperature XRD along with neutron diffraction and micro-Raman spectroscopy were used in

order to clarify such behavior in the two cobaltites. While many useful crystal lattice parameters along with vibrational behavior of the two ceramics were derived, the cause of high temperature stiffening of $LaCoO_3$ is still not clear. As the temperature was increased, lattice expansion was noticed in both cobaltites as expected. As the lattice expands, an increase in bond lengths was observed and as a result the bond strength is expected to decrease leading to a decrease in the effective Young's modulus for both $LaCoO_3$ and $La_{0.8}Ca_{0.2}CoO_3$. Yet, this is not the case with $LaCoO_3$ and thus more research is required to shed light on and find the exact physical phenomenon responsible for such tremendous increase in stiffness of this material. $LaCoO_3$ based perovskites have many applications as sensors [47], oxygen separation membranes [48], and in energy applications such as cathode material in solid oxide fuel cells [49] or as a catalyst in heterogeneous combustion [50]. The results from the current study will contribute to the understanding of the non-linear ferroelastic behavior of mixed ionic electronic conducting ceramics under thermo-mechanical loading.

ACKNOWLEDGEMENT

Funding: This work was supported by the National Science Foundation [grant numbers: 0968911, 1030833, 0748364]. A portion of this research at ORNL's High Flux Isotope Reactor and Spallation Neutron Source, was sponsored by the Scientific User Facilities Division, Office of Basic Energy Sciences, U.S. Department of Energy.

Figure captions

Figure 1. The stress-strain curve during uniaxial compressive loading and unloading for (A) $LaCoO_3$ and (B) $La_{0.8}Ca_{0.2}CoO_3$. The inset portions of the curves in the two figures show the initial portion of the stress-strain curve from uniaxial compressive loading (dotted line) plotted with stress-strain curve from 4-point bending for the two compounds.

Figure 2. Stress-strain curves obtained from four-point bending of $LaCoO_3$ during (A) heating from room temperature to 1000^{o}C and for (B) cooling back to room temperature. Similarly, stress-strain curves of $La_{0.8}Ca_{0.2}CoO_3$ during (C) heating from room temperature to 1000^{o}C and for (D) cooling back to room temperature.

Figure 3. The dependence of (A) hysteresis area, (C) irreversible strain, (E) maximum strain, and (G) elastic modulus with temperature in $LaCoO_3$ during mechanical loading and unloading; and the dependence of (B) hysteresis area, (D) irreversible strain, (F) maximum strain, and (H) elastic modulus with temperature in $La_{0.8}Ca_{0.2}CoO_3$. Solid circles correspond to heating, open circles correspond to cooling. Triangles are the values measured by Impulse Excitation Technique.

Figure 4. The diffraction patterns for LaCoO3 sample at or near room temperature from neutron diffraction at (A) High Flux Isotope Reactor, (B) Spallation Neutron Source and from (C) X-ray diffraction at High Temperature Materials Laboratory. The diffraction patterns for La0.8Ca0.2CoO3 sample at or near room temperature from neutron diffraction at (D) HFIR, (E) POWGEN and from (F) X-ray diffraction at High Temperature Materials Laboratory.

Figure 5. Schematic showing (A) the rhombohedral unit cell of $LaCoO_3$, space group $R\bar{3}C$, (B) hexagonal representation of the rhombohedral crystal structure, (C) the bond length and bond angle between Co and O atoms in the Co-O octahedron, (D) the bond length and bond angle between La and O atoms, (E) the Co-O-Co bond angle between adjacent octahedrons.

Figure 6. The change in diffraction patterns of $LaCoO_3$ and $La_{0.8}Ca_{0.2}CoO_3$ collected on different instruments during heating. The evolution of the single peak (024) and the doublet (006)/(202) in $LaCoO_3$ from the data collected at HFIR, POWGEN and HTML can be seen in (A), (B) and (C). Accordingly the evolution of the same peaks in $La_{0.8}Ca_{0.2}CoO_3$ are shown from the data collected at HFIR, POWGEN and HTML can be seen in (D), (E) and (F).

Figure 7. Neutron diffraction patterns after Rietveld refinement for $LaCoO_3$ from the data collected at HFIR for (A) 11^oC and (B) 1000^oC. Neutron diffraction patterns after Rietveld refinement for $La_{0.8}Ca_{0.2}CoO_3$ from the data collected at HFIR for (C) 11^oC and (D) 1000^oC. As can be seen, the calculated diffraction pattern (red line) matches well with the observed diffraction pattern (black cross markers) with minimal errors (blue line). The background (green line) is also seen to be fit well.

Figure 8. (A, B, C) Variation of lattice parameters and unit cell volume in rhombohedral system during heating and cooling of $LaCoO_3$ from the data collected via XRD at HTML, neutron diffraction at POWGEN and HFIR. (D, E, F) Variation of lattice parameters and unit cell volume in rhombohedral system during heating and cooling of $La_{0.8}Ca_{0.2}CoO_3$ from the data collected via XRD at HTML, neutron diffraction at POWGEN and HFIR.

Figure 9. (A, B, C) Change in Co-O bond length, O-Co-O bond angle and Co-O-Co bond angle during heating and cooling of $LaCoO_3$ from the data collected via neutron diffraction at POWGEN and HFIR. (D, E, F) Change in Co-O bond length, O-Co-O bond angle and Co-O-Co bond angle during heating and cooling of $La_{0.8}Ca_{0.2}CoO_3$ from the data collected via XRD at HTML, neutron diffraction at POWGEN and HFIR.

Figure 10. (A, B, C) Change in La-O bond length, O-La-O bond angle and the Geometric tolerance factor during heating and cooling of $LaCoO_3$ from the data collected neutron diffraction at

POWGEN and HFIR. (D, E, F) Change in La-O bond length, O-La-O bond angle and the Geometric tolerance factor during heating and cooling of $La_{0.8}Ca_{0.2}CoO_3$ from the data collected via XRD at HTML, neutron diffraction at POWGEN and HFIR.

Figure 11. Neutron diffraction data from POWGEN and HFIR. (A, B) shows the change in the oxygen occupancy in the unit cell during heating of $LaCoO_3$ and $La_{0.8}Ca_{0.2}CoO_3$ respectively. (C, D) shows the change in the atomic displacement parameter (U_{iso}) for the oxygen atom during heating of $LaCoO_3$ and $La_{0.8}Ca_{0.2}CoO_3$ respectively. The slope of the trend line for $LaCoO_3$ up to 500°C is $3x10^{-5}$ and then changes to $4x10^{-5}$ from 600°C to 900°C (C). The slope of the trend line for $La_{0.8}Ca_{0.2}CoO_3$ remains at $4x10^{-5}$ up to 900°C (D).

Figure 12. Raman spectra collected for $LaCoO_3$ as it is heated from room temperature to 900°C and then cooled back to room temperature. 1 – 160 cm^{-1}, 2 – 185 cm^{-1}, 3' – 400 cm^{-1}, 3 – 450 cm^{-1}, 4 – 550 cm^{-1}, 5 – 700 cm^{-1}.

Figure 13. Raman spectra collected for $La_{0.8}Ca_{0.2}CoO_3$ as it is heated from room temperature to 900°C and then cooled back to room temperature. 1 – 160 cm^{-1}, 2 – 185 cm^{-1}, 3 – 400 cm^{-1}, 4 – 450 cm^{-1}, 5 – 550 cm^{-1}, 6 – 700 cm^{-1}.

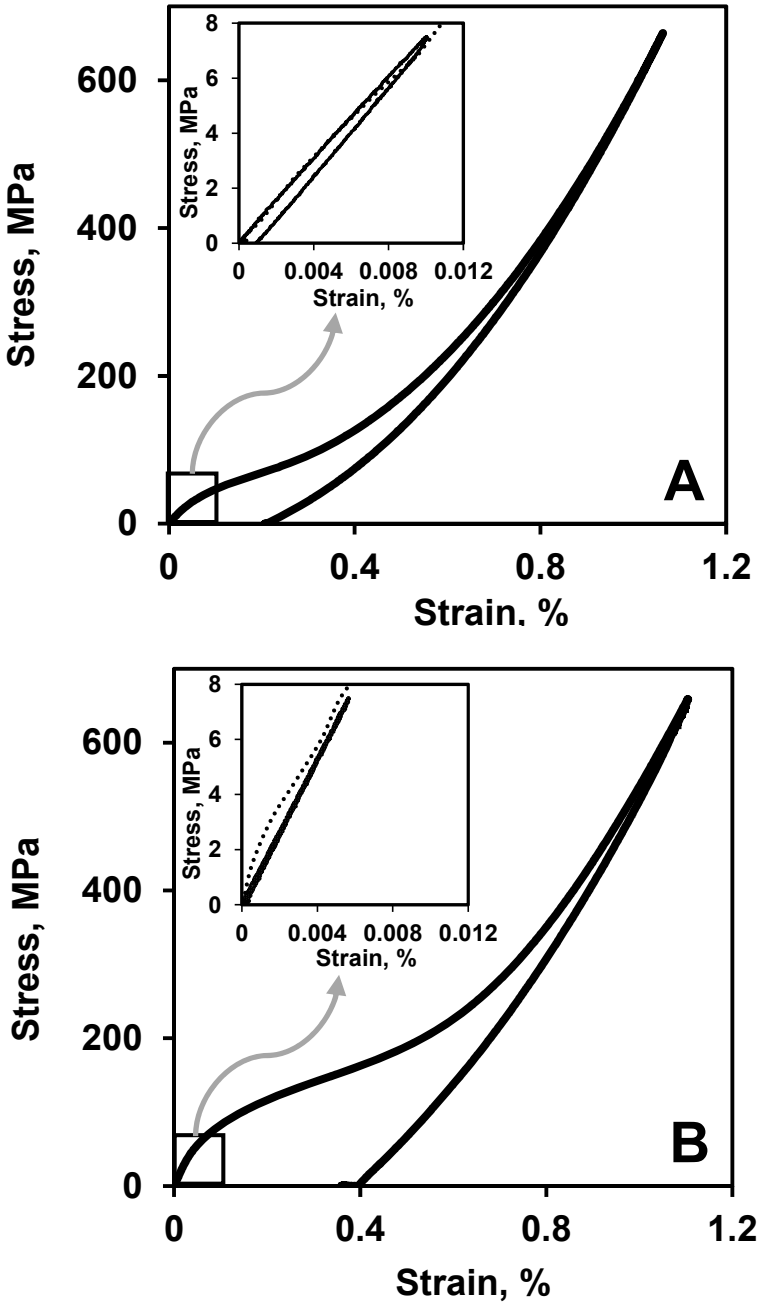

Figure 1. Stress-strain curve during uniaxial compressive loading and unloading for (A) $LaCoO_3$ and (B) $La_{0.8}Ca_{0.2}CoO_3$. The inset portions of the curves in the two figures show the initial portion

of the stress-strain curve from uniaxial compressive loading (dotted line) plotted with stress-strain curve from 4-point bending for the two compounds.

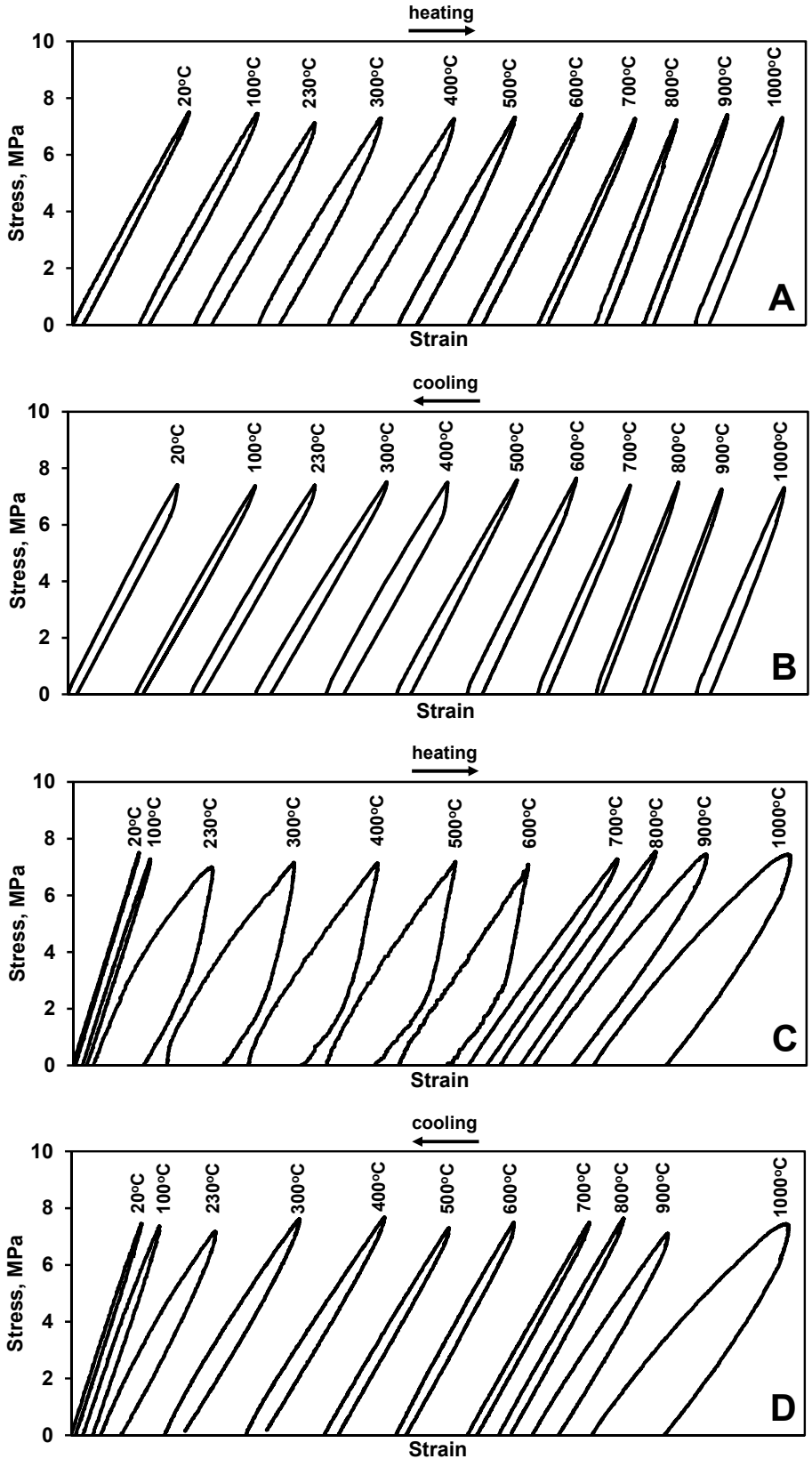
heating
20°C
100°C
230°C
300°C
400°C
500°C
600°C
700°C
800°C
900°C
1000°C
Stress, MPa
Strain
A
cooling
B
heating
C
cooling
D

Figure 2. Stress-strain curves obtained from four-point bending of $LaCoO_3$ during (A) heating from room temperature to 1000ºC and for (B) cooling back to room temperature. Similarly, stress-strain curves of $La_{0.8}Ca_{0.2}CoO_3$ during (C) heating from room temperature to 1000ºC and for (D) cooling back to room temperature.

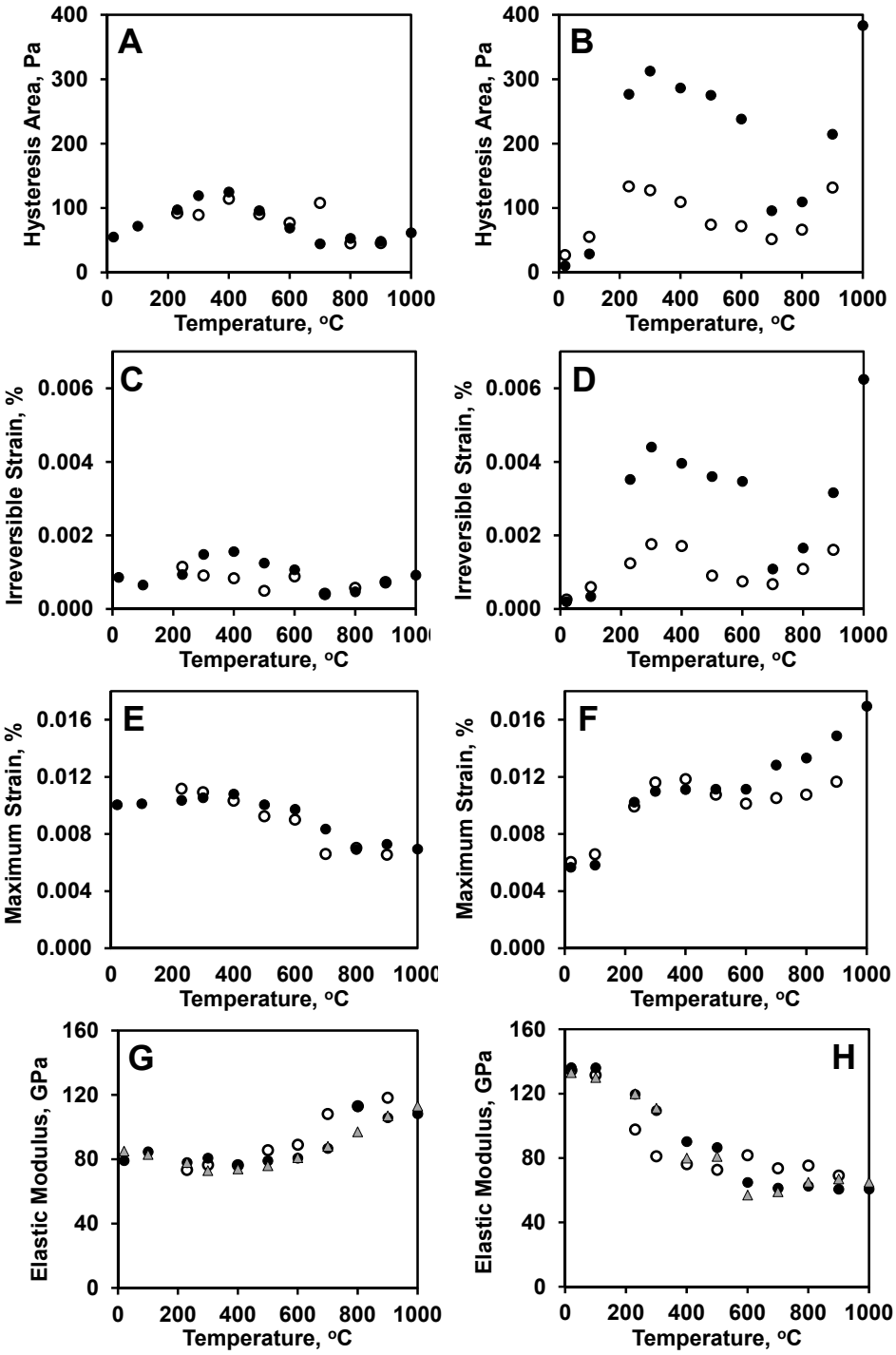

Figure 3. The dependence of (A) hysteresis area, (C) irreversible strain, (E) maximum strain, and (G) elastic modulus with temperature in $LaCoO_3$ during mechanical loading and unloading; and the dependence of (B) hysteresis area, (D) irreversible strain, (F) maximum strain, and (H) elastic

modulus with temperature in $La_{0.8}Ca_{0.2}CoO_3$. Solid circles correspond to heating, open circles correspond to cooling. Triangles are the values measured by Impulse Excitation Technique.

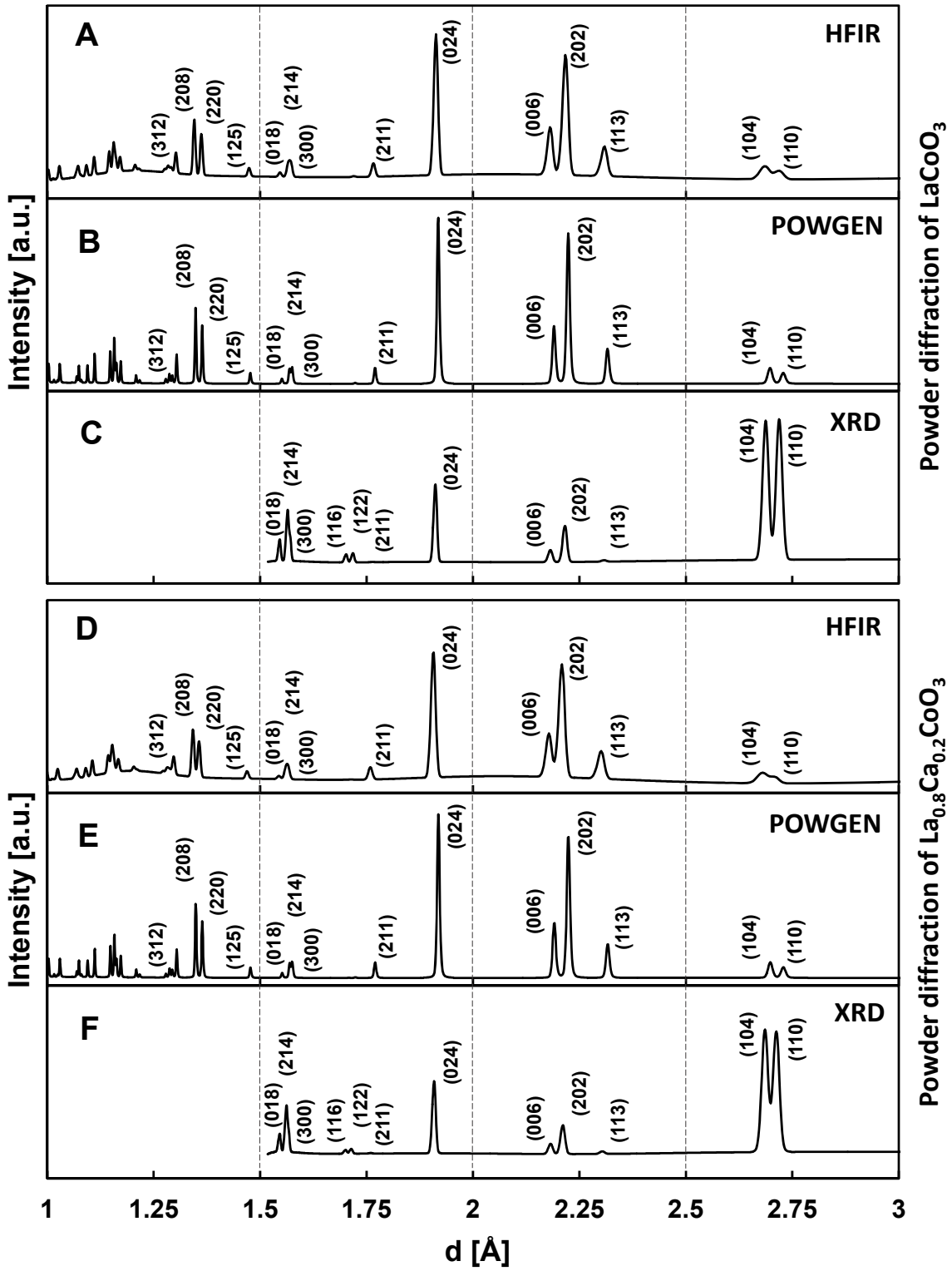
A
HFIR
B
POWGEN
C
XRD
D
HFIR
E
POWGEN
F
XRD
(312)
(208)
(220)
(125)
(018)
(214)
(300)
(211)
(024)
(006)
(202)
(113)
(104)
(110)
(116)
(122)
Intensity [a.u.]
Powder diffraction of LaCoO3 at room temperature
Powder diffraction of La0.8Ca0.2CoO3 at room temperature
1
1.25
1.5
1.75
2
2.25
2.5
2.75
3
d [Å]

Figure 4. The diffraction patterns for $LaCoO_3$ sample at or near room temperature from neutron diffraction at (A) High Flux Isotope Reactor, (B) Spallation Neutron Source and from (C) X-ray diffraction at High Temperature Materials Laboratory. The diffraction patterns for $La_{0.8}Ca_{0.2}CoO_3$ sample at or near room temperature from neutron diffraction at (D) HFIR, (E) POWGEN and from (F) X-ray diffraction at High Temperature Materials Laboratory.

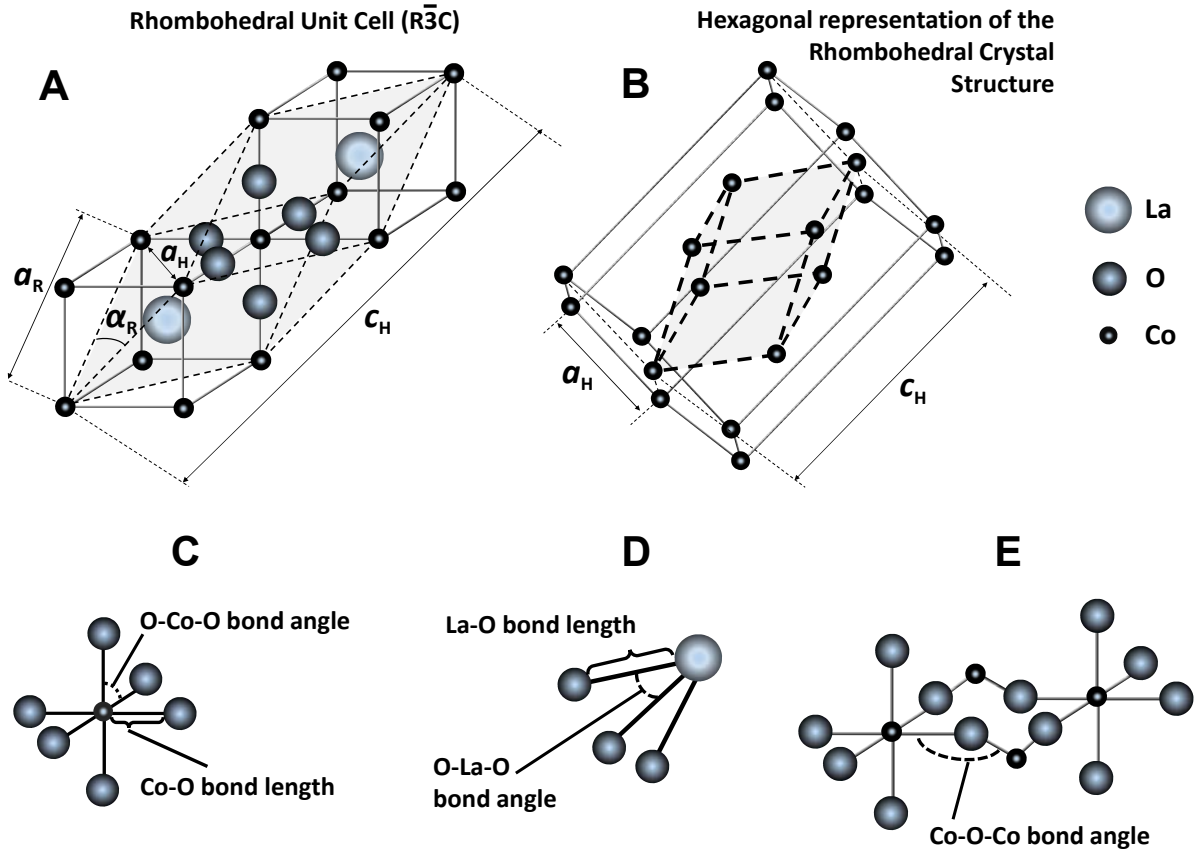

Figure 5. Schematic showing (A) the rhombohedral unit cell of $LaCoO_3$, space group $R\bar{3}C$, (B) hexagonal representation of the rhombohedral crystal structure, (C) the bond length and bond angle between Co and O atoms in the Co-O octahedron, (D) the bond length and bond angle between La and O atoms, (E) the Co-O-Co bond angle between adjacent octahedrons.

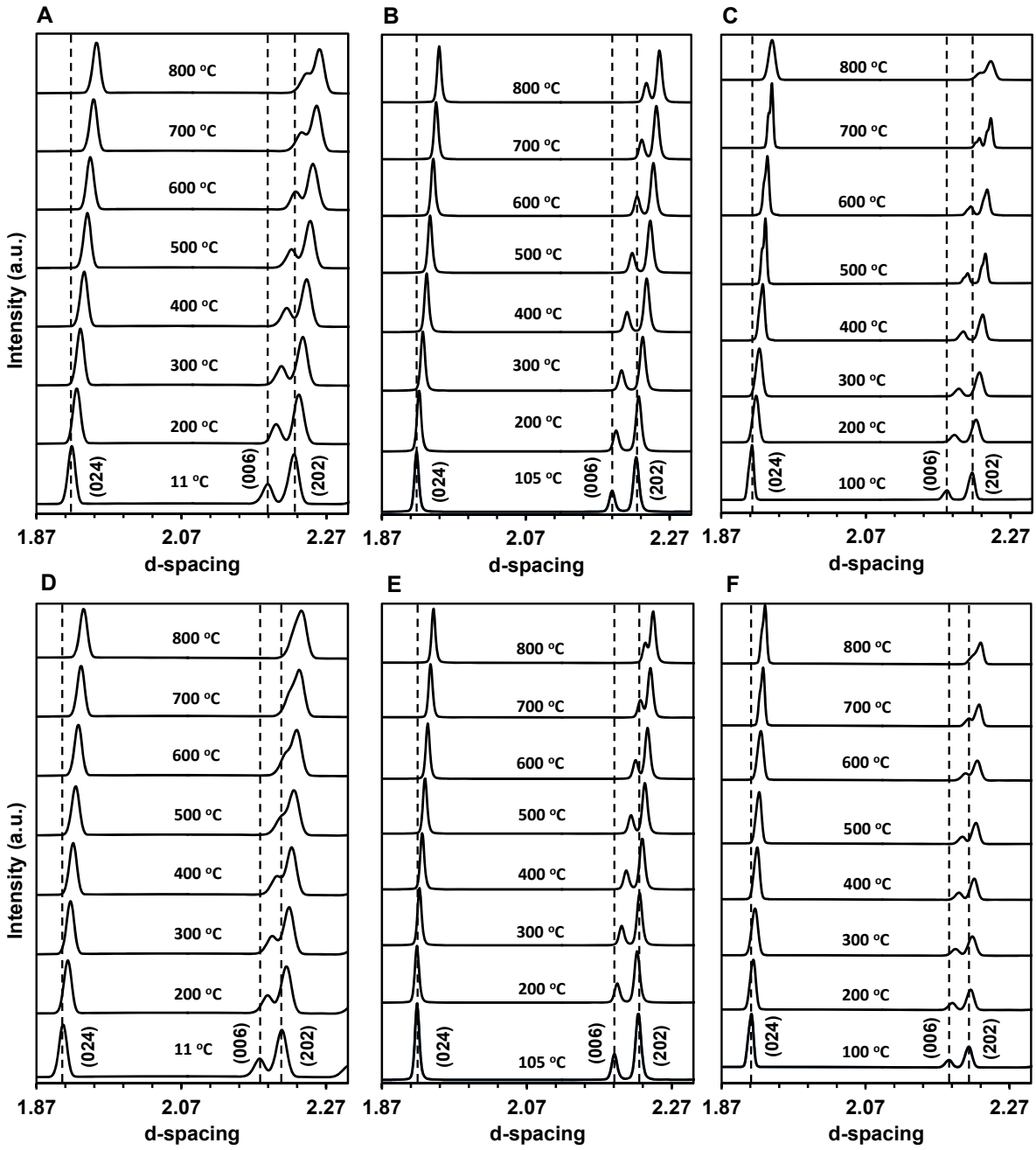

Figure 6. The change in diffraction patterns of $LaCoO_3$ and $La_{0.8}Ca_{0.2}CoO_3$ collected on different instruments during heating. The evolution of the single peak (024) and the doublet (006)/(202) in $LaCoO_3$ from the data collected at HFIR, POWGEN and HTML can be seen in (A), (B) and (C).

Accordingly the evolution of the same peaks in $La_{0.8}Ca_{0.2}CoO_3$ are shown from the data collected at HFIR, POWGEN and HTML can be seen in (D), (E) and (F).

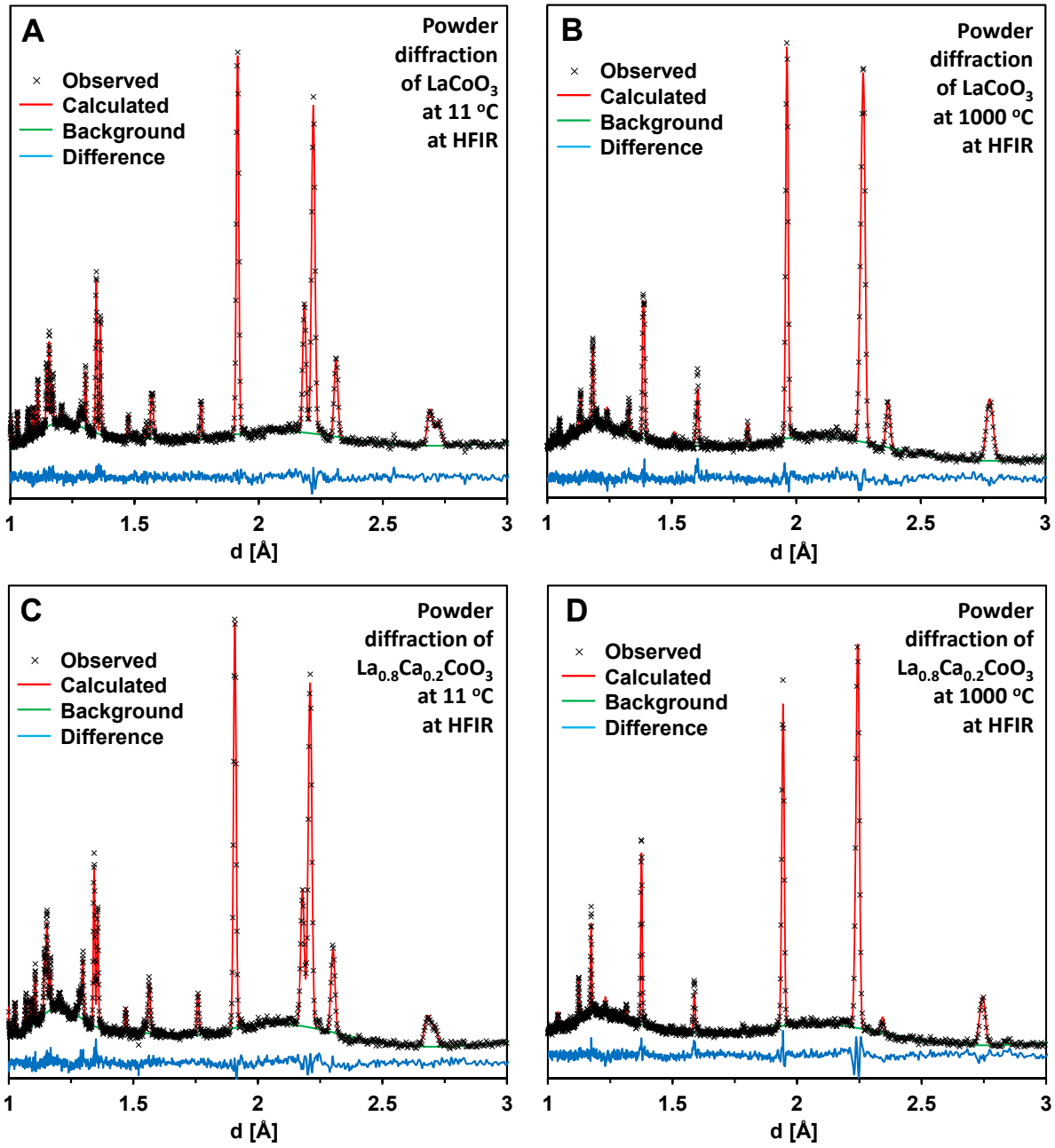

Figure 7. Neutron diffraction patterns after Rietveld refinement for $LaCoO_3$ from the data collected at HFIR for (A) 11°C and (B) 1000°C. Neutron diffraction patterns after Rietveld refinement for $La_{0.8}Ca_{0.2}CoO_3$ from the data collected at HFIR for (C) 11°C and (D) 1000°C. As can be seen, the calculated diffraction pattern (red line) matches well with the observed diffraction pattern (black

cross markers) with minimal errors (blue line). The background (green line) is also seen to be fit well.

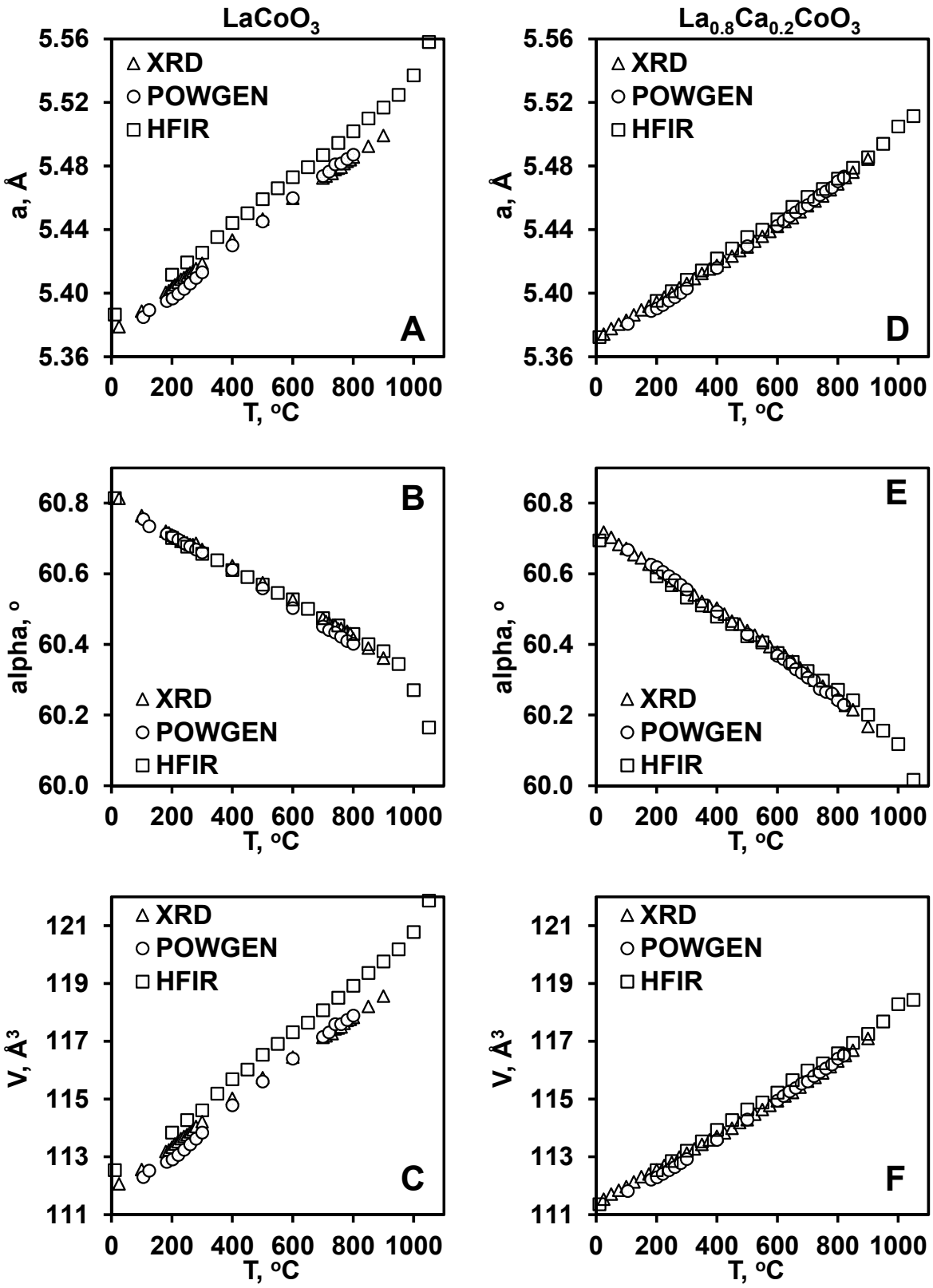
LaCoO3
La0.8Ca0.2CoO3
XRD
POWGEN
HFIR
a, Å
alpha, °
V, Å3
T, °C
A
B
C
D
E
F

Figure 8. (A, B, C) Variation of lattice parameters and unit cell volume in rhombohedral system during heating and cooling of $LaCoO_3$ from the data collected via XRD at HTML, neutron diffraction at POWGEN and HFIR. (D, E, F) Variation of lattice parameters and unit cell volume in rhombohedral system during heating and cooling of $La_{0.8}Ca_{0.2}CoO_3$ from the data collected via XRD at HTML, neutron diffraction at POWGEN and HFIR.

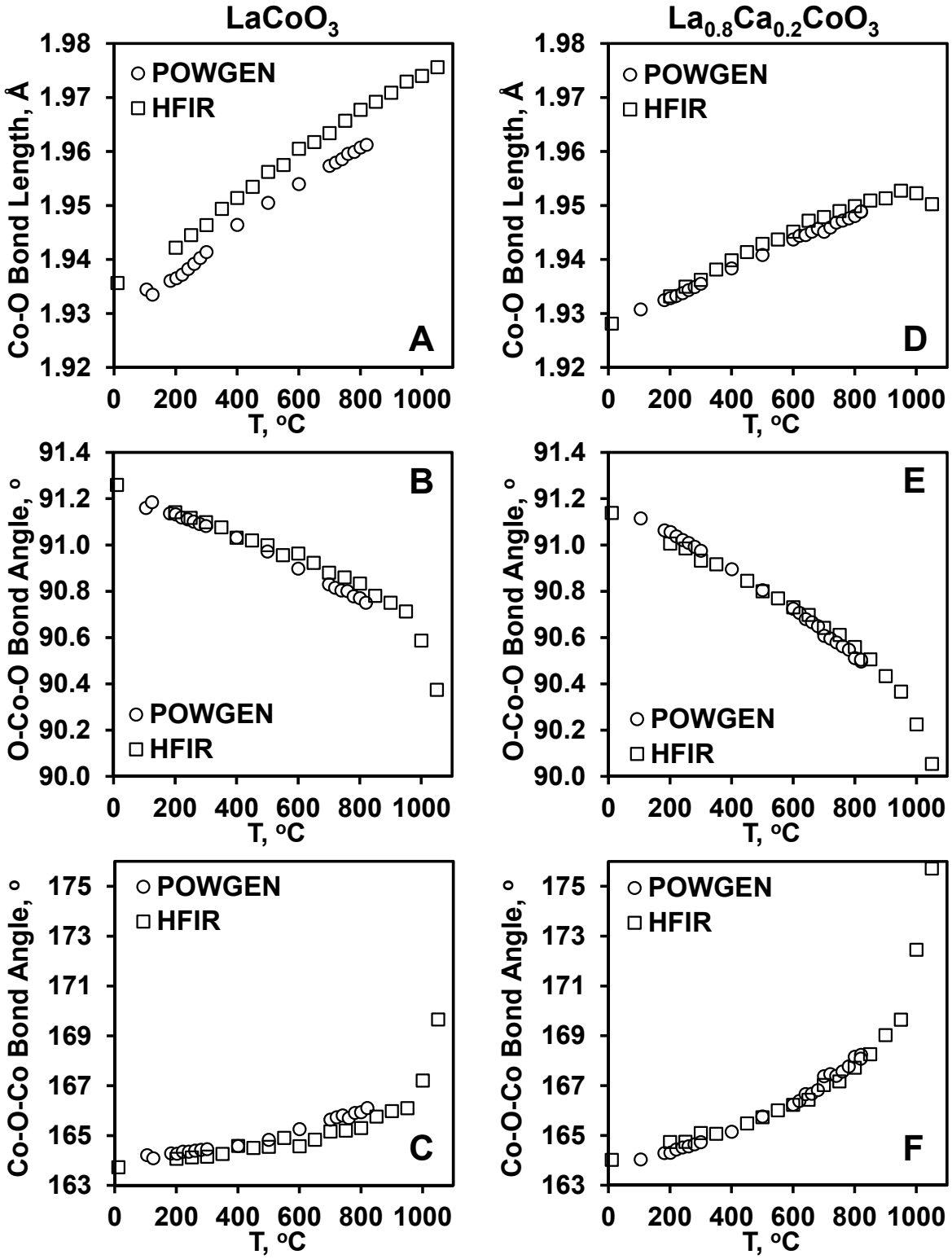
LaCoO3
La0.8Ca0.2CoO3
POWGEN
HFIR
Co-O Bond Length, Å
O-Co-O Bond Angle, °
Co-O-Co Bond Angle, °
T, °C
A
B
C
D
E
F

Figure 9. (A, B, C) Change in Co-O bond length, O-Co-O bond angle and Co-O-Co bond angle during heating and cooling of $LaCoO_3$ from the data collected via neutron diffraction at POWGEN and HFIR. (D, E, F) Change in Co-O bond length, O-Co-O bond angle and Co-O-Co bond angle during heating and cooling of $La_{0.8}Ca_{0.2}CoO_3$ from the data collected via XRD at HTML, neutron diffraction at POWGEN and HFIR.

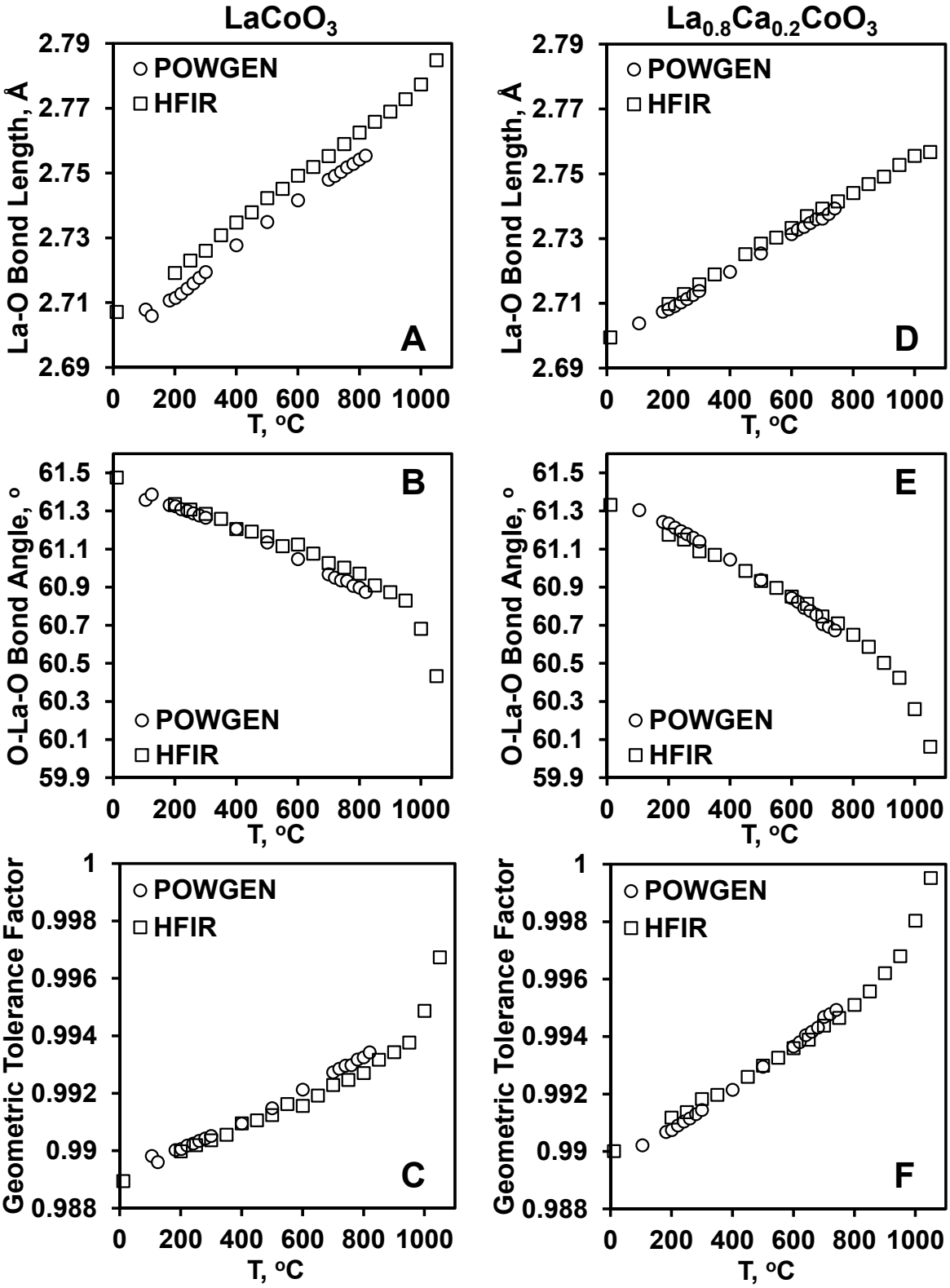
LaCoO3
La0.8Ca0.2CoO3
POWGEN
HFIR
La-O Bond Length, Å
O-La-O Bond Angle, °
Geometric Tolerance Factor
T, °C
A
B
C
D
E
F

Figure 10. (A, B, C) Change in La-O bond length, O-La-O bond angle and the Geometric tolerance factor during heating and cooling of $LaCoO_3$ from the data collected neutron diffraction at POWGEN and HFIR. (D, E, F) Change in La-O bond length, O-La-O bond angle and the Geometric tolerance factor during heating and cooling of $La_{0.8}Ca_{0.2}CoO_3$ from the data collected via XRD at HTML, neutron diffraction at POWGEN and HFIR.

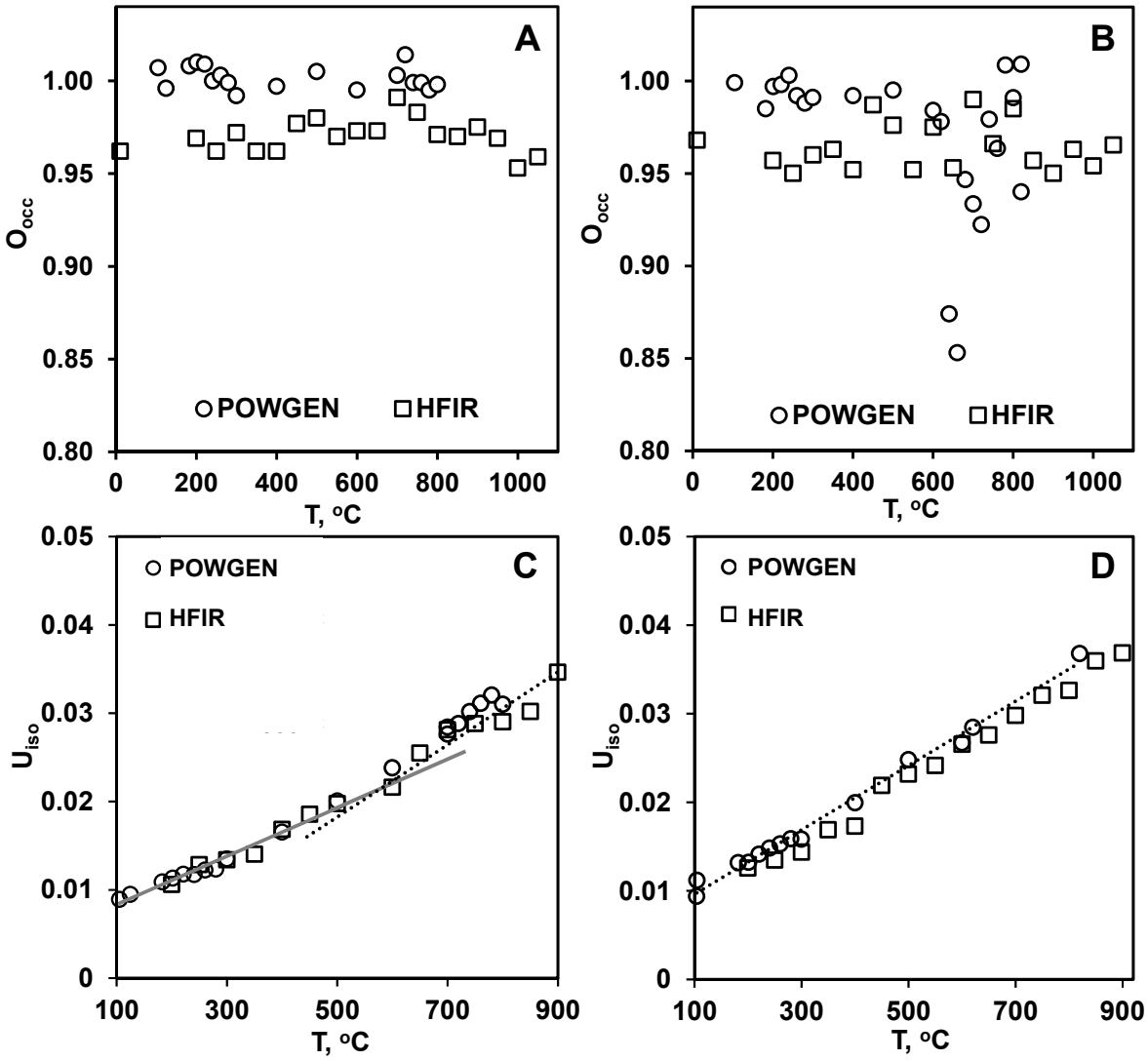

Figure 11. Neutron diffraction data from POWGEN and HFIR. (A, B) shows the change in the oxygen occupancy in the unit cell during heating of $LaCoO_3$ and $La_{0.8}Ca_{0.2}CoO_3$ respectively. (C, D) shows the change in the atomic displacement parameter (U_{iso}) for the oxygen atom during heating of $LaCoO_3$ and $La_{0.8}Ca_{0.2}CoO_3$ respectively. The slope of the trend line for $LaCoO_3$ up to 500°C is $3x10^{-5}$ and then changes to $4x10^{-5}$ from 600°C to 900°C (C). The slope of the trend line for $La_{0.8}Ca_{0.2}CoO_3$ remains at $4x10^{-5}$ up to 900°C (D).

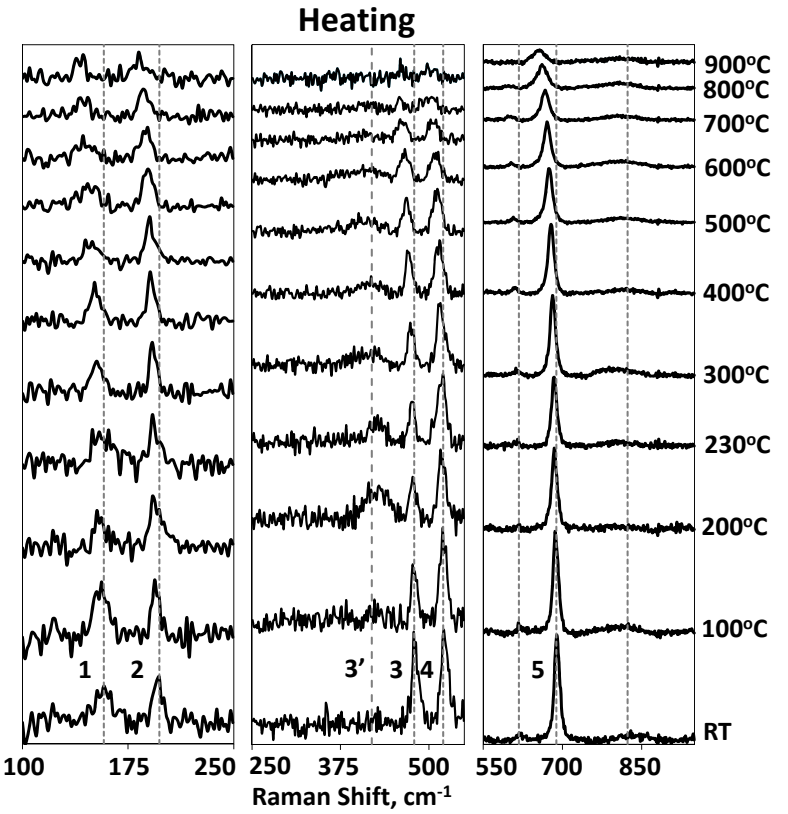
Heating
900°C
800°C
700°C
600°C
500°C
400°C
300°C
230°C
200°C
100°C
RT
1
2
3'
3
4
5
100
175
250
250
375
500
550
700
850
Raman Shift, cm-1

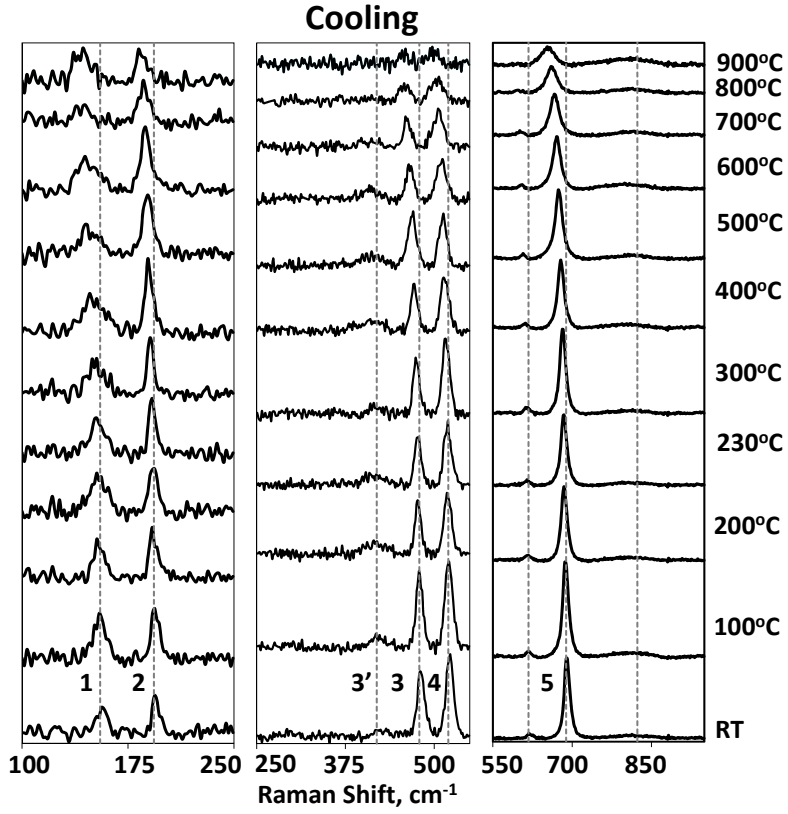
Cooling
900°C
800°C
700°C
600°C
500°C
400°C
300°C
230°C
200°C
100°C
RT
1
2
3'
3
4
5
100
175
250
250
375
500
550
700
850
Raman Shift, cm-1

Figure 12. Raman spectra collected for $LaCoO_3$ as it is heated from room temperature to 900ºC and then cooled back to room temperature. 1 – 160 cm^{-1}, 2 – 185 cm^{-1}, 3' – 400 cm^{-1}, 3 – 450 cm^{-1}, 4 – 550 cm^{-1}, 5 – 700 cm^{-1}.

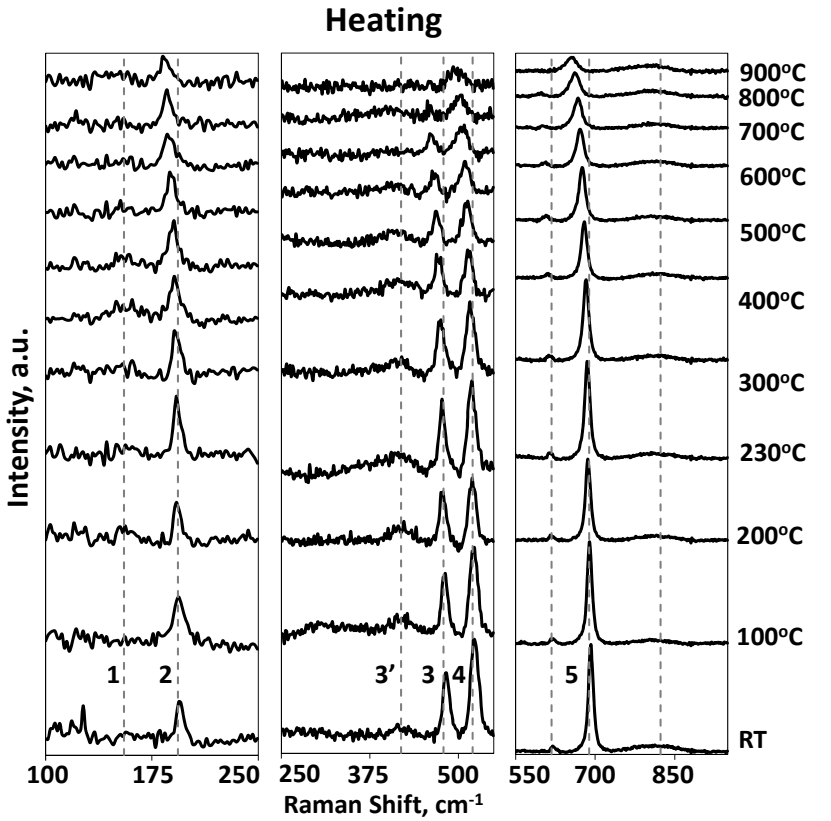
Heating
Intensity, a.u.
900°C
800°C
700°C
600°C
500°C
400°C
300°C
230°C
200°C
100°C
RT
1
2
3'
3
4
5
100
175
250
250
375
500
550
700
850
Raman Shift, cm-1

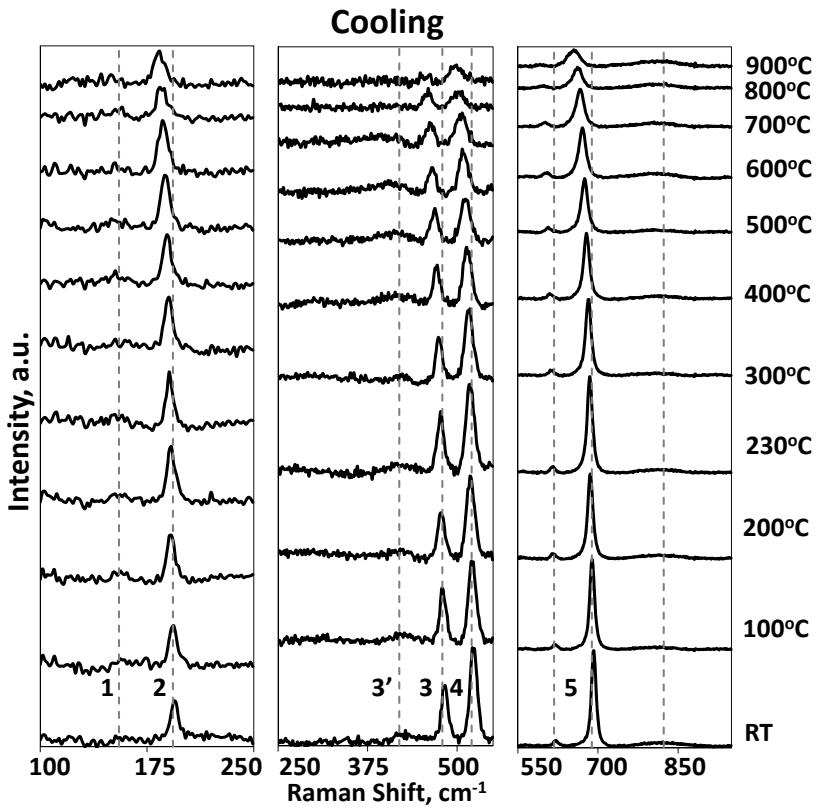
Cooling
Intensity, a.u.
900°C
800°C
700°C
600°C
500°C
400°C
300°C
230°C
200°C
100°C
RT
1
2
3'
3
4
5
100
175
250
250
375
500
550
700
850
Raman Shift, cm-1

Figure 13. Raman spectra collected for $La_{0.8}Ca_{0.2}CoO_3$ as it is heated from room temperature to 900°C and then cooled back to room temperature. 1 – 160 cm^{-1}, 2 – 185 cm^{-1}, 3 – 400 cm^{-1}, 4 – 450 cm^{-1}, 5 – 550 cm^{-1}, 6 – 700 cm^{-1}.

REFERENCES

[1] J.B. Goodenough, Narrow-band electrons in transition-metal oxides, Czechoslovak Journal of Physics B 17(4) (1967) 304-336.
[2] K. Huang, M. Feng, J.B. Goodenough, M. Schmerling, Characterization of Sr-Doped $LaMnO_3$ and $LaCoO_3$ as Cathode Materials for a Doped $LaGaO_3$ Ceramic Fuel Cell, Journal of the Electrochemical Society 143(11) (1996) 3630-3636.
[3] J. Stevenson, T. Armstrong, R. Carneim, L.R. Pederson, W. Weber, Electrochemical Properties of Mixed Conducting Perovskites $La_{1-x}M_xCo_{1-y}Fe_yO_{3-\delta}$ (M= Sr, Ba, Ca), Journal of the Electrochemical Society 143(9) (1996) 2722-2729.
[4] V. Kharton, F. Figueiredo, A. Kovalevsky, A. Viskup, E. Naumovich, A. Yaremchenko, I. Bashmakov, F. Marques, Processing, microstructure and properties of $LaCoO_{3-\delta}$ ceramics, Journal of the European Ceramic Society 21(13) (2001) 2301-2309.
[5] L. Simonot, G. Maire, A comparative study of $LaCoO_3$, Co_3O_4 and $LaCoO_3$—Co_3O_4: I. Preparation, characterisation and catalytic properties for the oxidation of CO, Applied Catalysis B: Environmental 11(2) (1997) 167-179.
[6] S. Royer, F. Berube, S. Kaliaguine, Effect of the synthesis conditions on the redox and catalytic properties in oxidation reactions of $LaCo_{1-x}Fe_xO_3$, Applied Catalysis A: General 282(1) (2005) 273-284.
[7] N. Orlovskaya, K. Kleveland, T. Grande, M.-A. Einarsrud, Mechanical properties of $LaCoO_3$ based ceramics, Journal of the European Ceramic Society 20(1) (2000) 51-56.
[8] N. Orlovskaya, Y. Gogotsi, M. Reece, B. Cheng, I. Gibson, Ferroelasticity and hysteresis in $LaCoO_3$ based perovskites, Acta materialia 50(4) (2002) 715-723.
[9] A. Aman, Y. Chen, M. Lugovy, N. Orlovskaya, M.J. Reece, D. Ma, A.D. Stoica, K. An, In-situ neutron diffraction of $LaCoO_3$ perovskite under uniaxial compression. I. Crystal structure analysis and texture development, Journal of Applied Physics 116(1) (2014) 013503.
[10] M. Lugovy, A. Aman, Y. Chen, N. Orlovskaya, J. Kuebler, T. Graule, M.J. Reece, D. Ma, A.D. Stoica, K. An, In-situ neutron diffraction of LaCoO3 perovskite under uniaxial compression. II. Elastic properties, Journal of Applied Physics 116(1) (2014) 013504.
[11] N. Orlovskaya, M. Lugovy, S. Pathak, D. Steinmetz, J. Lloyd, L. Fegely, M. Radovic, E.A. Payzant, E. Lara-Curzio, L.F. Allard, Thermal and mechanical properties of $LaCoO_3$ and $La_{0.8}Ca_{0.2}CoO_3$ perovskites, Journal of Power Sources 182(1) (2008) 230-239.
[12] M. Senarıs-Rodrıguez, J. Goodenough, $LaCoO_3$ revisited, Journal of Solid State Chemistry 116(2) (1995) 224-231.
[13] G. Thornton, B. Tofield, A. Hewat, A neutron diffraction study of $LaCoO_3$ in the temperature range 4.2< T< 1248 K, Journal of Solid State Chemistry 61(3) (1986) 301-307.
[14] J. Mastin, M.-A. Einarsrud, T. Grande, Structural and Thermal Properties of $La_{1-x}Sr_xCoO_{3-\delta}$, Chemistry of materials 18(25) (2006) 6047-6053.
[15] G. Maris, Y. Ren, V. Volotchaev, C. Zobel, T. Lorenz, T. Palstra, Evidence for orbital ordering in $LaCoO_3$, Physical Review B 67(22) (2003) 224423.
[16] V. Gnezdilov, K.-Y. Choi, Y. Pashkevich, P. Lemmens, S. Shiryaev, G. Bychkov, S. Barilo, V. Fomin, A. Yeremenko, Low temperature mixed spin state of Co^{3+} in $LaCoO_3$ evidenced from Jahn-Teller lattice distortions, arXiv preprint cond-mat/0601121 (2006).
[17] Y. Wang, H.J. Fan, Orbital ordering-driven ferromagnetism in $LaCoO_3$ nanowires, Journal of Applied Physics 108(5) (2010) 3917.
[18] P.E. Vullum, R. Holmestad, H.L. Lein, J. Mastin, M.A. Einarsrud, T. Grande, Monoclinic Ferroelastic Domains in $LaCoO_3$-Based Perovskites, Advanced Materials 19(24) (2007) 4399-4403.

[19] P.E. Vullum, H.L. Lein, M.-A. Einarsrud, T. Grande, R. Holmestad, TEM observations of rhombohedral and monoclinic domains in LaCoO3-based ceramics, Philosophical Magazine 88(8) (2008) 1187-1208.
[20] P. Raccah, J. Goodenough, First-Order Localized-Electron⇆Collective-Electron Transition in LaCo O 3, Physical Review 155(3) (1967) 932.
[21] Y. Kimura, Mechanical Properties of Perovskite and Related Oxides for Energy Conversion Devices, Graduate School of Environmental Studies, Tohoku University, Japan, 2015.
[22] S. Giraud, J. Canel, Young's modulus of some SOFCs materials as a function of temperature, Journal of the European Ceramic Society 28(1) (2008) 77-83.
[23] A. Julian, E. Juste, P.-M. Geffroy, N. Tessier-Doyen, P. Del Gallo, N. Richet, T. Chartier, Thermal behaviour of $La_{0.8}Sr_{0.2}Fe_{1-x}Ga_xO_{3-\delta}$ (x= 0 or x= 0.3), Journal of the European Ceramic Society 29(12) (2009) 2603-2610.
[24] E. Sánchez-González, P. Miranda, J.J. Meléndez-Martínez, F. Guiberteau, A. Pajares, Temperature dependence of mechanical properties of alumina up to the onset of creep, Journal of the European Ceramic Society 27(11) (2007) 3345-3349.
[25] L. Dong, D.S. Stone, R.S. Lakes, Softening of bulk modulus and negative Poisson ratio in barium titanate ceramic near the Curie point, Philosophical Magazine Letters 90(1) (2010) 23-33.
[26] T. Okamura, S. Shimizu, M. Mogi, M. Tanimura, K. Furuya, F. Munakata, Elastic properties of Sr-and Mg-doped lanthanum gallate at elevated temperature, Journal of power sources 130(1) (2004) 38-41.
[27] Y. Zou, W. Araki, M. Balaguer, J. Malzbender, Elastic properties of freeze-cast $La_{0.6}Sr_{0.4}Co_{0.2}Fe_{0.8}O_{3-\delta}$, Journal of the European Ceramic Society 36(7) (2016) 1651-1657.
[28] W. Araki, Y. Arai, J. Malzbender, Transitions of $Ba_{0.5}Sr_{0.5}Co_{0.8}Fe_{0.2}O_{3-\delta}$ and $La_{0.58}Sr_{0.4}Co_{0.2}Fe_{0.8}O_{3-\delta}$, Materials letters 132 (2014) 295-297.
[29] CEN, EN 843-1, Part 1: Determination of Flexural Strength, EUROPEAN COMMITTEE FOR STANDARDIZATION, Brussels, Belgium, 2006.
[30] CEN, EN 843-2, Part 2: Determination of Young's modulus, shear modulus and Poisson's ratio, EUROPEAN COMMITTEE FOR STANDARDIZATION, Brussels, Belgium, 2006.
[31] A. Larson, R. Von Dreele, GSAS: generalized structure analysis system, Document LAUR (1994) 86-748.
[32] B.H. Toby, EXPGUI, a graphical user interface for GSAS, Journal of applied crystallography 34(2) (2001) 210-213.
[33] K. Kleveland, N. Orlovskaya, T. Grande, A.M. Moe, M.A. Einarsrud, K. Breder, G. Gogotsi, Ferroelastic Behavior of $LaCoO_3$-Based Ceramics, J. Am. Ceram. Soc. 84(9) (2001) 2029-2033.
[34] N. Orlovskaya, N. Browning, A. Nicholls, Ferroelasticity in mixed conducting $LaCoO_3$ based perovskites: a ferroelastic phase transition, Acta materialia 51(17) (2003) 5063-5071.
[35] P.G. Radaelli, S.-W. Cheong, Structural phenomena associated with the spin-state transition in $LaCoO_3$, Physical Review B 66(9) (2002) 094408.
[36] D. Kozlenko, N. Golosova, Z. Jirak, L. Dubrovinsky, B. Savenko, M. Tucker, Y. Le Godec, V. Glazkov, Temperature-and pressure-driven spin-state transitions in $LaCoO_3$, Physical Review B 75(6) (2007) 064422.
[37] Z. Zhang, J. Koppensteiner, W. Schranz, D. Prabhakaran, M.A. Carpenter, Strain coupling mechanisms and elastic relaxation associated with spin state transitions in $LaCoO_3$, Journal of Physics: Condensed Matter 23(14) (2011) 145401.
[38] K. Knížek, Z. Jirák, J. Hejtmánek, M. Veverka, M. Maryško, G. Maris, T. Palstra, Structural anomalies associated with the electronic and spin transitions in $LnCoO_3$, The European Physical Journal B-Condensed Matter and Complex Systems 47(2) (2005) 213-220.
[39] P.G. Radaelli, M. Marezio, H.Y. Hwang, S.W. Cheong, B. Batlogg, Charge localization by static and dynamic distortions of the CoO_6 octahedra in perovskite manganites, Physical Review B 54(13) (1996) 8992-8995.

[40] M. Abrashev, A. Litvinchuk, M. Iliev, R. Meng, V. Popov, V. Ivanov, R. Chakalov, C. Thomsen, Comparative study of optical phonons in the rhombohedrally distorted perovskites $LaAlO_3$ and $LaMnO_3$, Physical Review B 59(6) (1999) 4146.
[41] N. Orlovskaya, D. Steinmetz, S. Yarmolenko, D. Pai, J. Sankar, J. Goodenough, Detection of temperature-and stress-induced modifications of $LaCoO_3$ by micro-Raman spectroscopy, Physical Review B 72(1) (2005) 014122.
[42] A. Aman, R. Stadelmann, N. Orlovskaya, High temperature study of $LaCoO_3$ based perovskites by micro-Raman spectroscopy, University of Central Florida, 2016.
[43] W. Araki, J. Malzbender, Ferroelastic deformation of $La_{0.58}Sr_{0.4}Co_{0.2}Fe_{0.8}O_{3-\delta}$ under uniaxial compressive loading, Journal of the European Ceramic Society 33(4) (2013) 805-812.
[44] E.K. Salje, H. Zhang, Domain boundary pinning and elastic softening in $KMnF_3$ and $KMn_{1-x}Ca_xF_3$, Journal of Physics: Condensed Matter 21(3) (2008) 035901.
[45] R.J. Harrison, S.A. Redfern, J. Street, The effect of transformation twins on the seismic-frequency mechanical properties of polycrystalline $Ca_{1-x}Sr_xTiO_3$ perovskite, American Mineralogist 88(4) (2003) 574-582.
[46] W. Lee, E. Salje, U. Bismayer, Influence of point defects on the distribution of twin wall widths, Physical Review B 72(10) (2005) 104116.
[47] J.-C. Ding, H.-Y. Li, Z.-X. Cai, X.-D. Zhang, X. Guo, $LaCoO_3$-based sensors with high sensitivity to carbon monoxide, RSC Advances 5(81) (2015) 65668-65673.
[48] J. Sunarso, S. Baumann, J. Serra, W. Meulenberg, S. Liu, Y. Lin, J.D. Da Costa, Mixed ionic–electronic conducting (MIEC) ceramic-based membranes for oxygen separation, Journal of Membrane Science 320(1) (2008) 13-41.
[49] K. Huang, H.Y. Lee, J.B. Goodenough, Sr-and Ni-Doped $LaCoO_3$ and $LaFeO_3$ Perovskites New Cathode Materials for Solid-Oxide Fuel Cells, Journal of the Electrochemical Society 145(9) (1998) 3220-3227.
[50] A. C. Terracciano, N. Orlovskaya, $LaCoO_3$ Catalytically Enhanced MgO Partially Stabilized Zirconia in Heterogeneous Methane Combustion, University of Central Florida, 2016.